

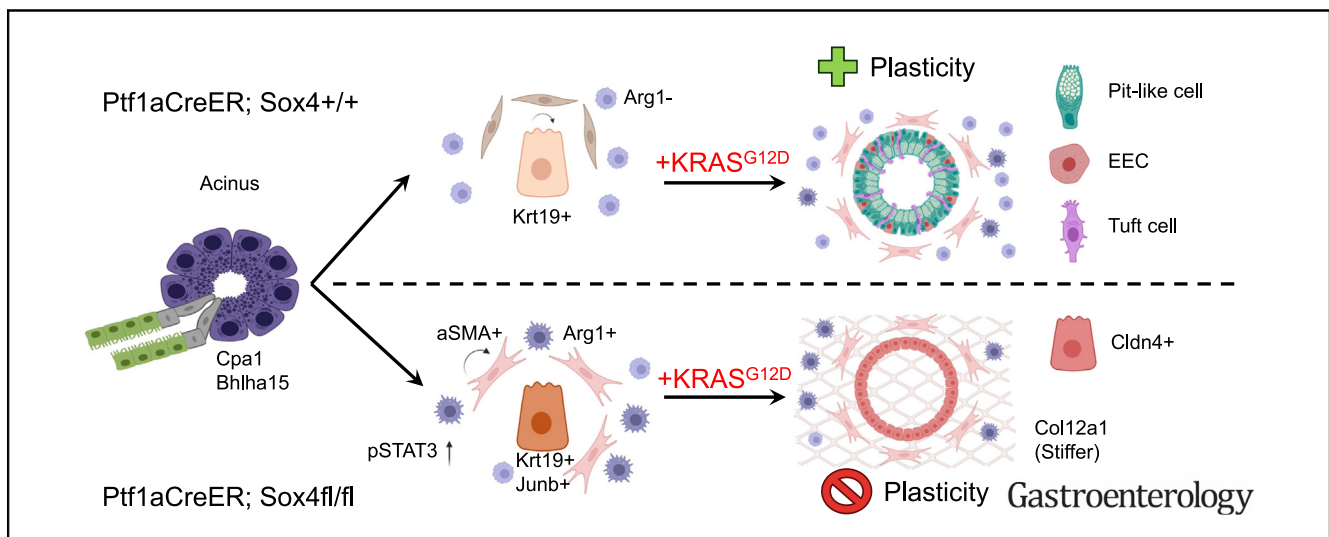
PANCREAS

Resolution of Acinar Dedifferentiation Regulates Tissue Remodeling in Pancreatic Injury and Cancer Initiation



Jonathan Baldan,^{1,6,*} Juan Camacho-Roda,^{1,*} Marta Ballester,^{1,*} Kristina Høj,¹ Anita Kurilla,¹ H. Carlo Maurer,² Sebastian Arcila-Barrera,³ Xinyi Lin,^{4,5} Zhaolong Pan,⁶ Joana Leitão Castro,¹ Alejandro Enrique Mayorca-Guilliani,¹ Charlotte Vestrup Rift,⁷ Jane Hasselby,⁷ Luc Bouwens,⁸ Véronique Lefebvre,⁹ Charles J. David,^{4,5} Oren Parnas,³ Kathleen E. DelGiorno,¹⁰ Janine Terra Erler,¹ Ilse Roman,⁶ and Luis Arnes¹

¹Biotech Research and Innovation Centre, University of Copenhagen, Copenhagen, Denmark; ²Department of Internal Medicine II, Technical University of Munich, Munich, Germany; ³The Lautenberg Center for Immunology and Cancer Research, The Hebrew University of Jerusalem, Jerusalem, Israel; ⁴Tsinghua University School of Medicine, Beijing, China; ⁵Peking University–Tsinghua Center for Life Sciences, Beijing, China; ⁶Translational Oncology Research Center, Vrije Universiteit Brussel, Brussels, Belgium; ⁷Department of Pathology, Copenhagen University Hospital Rigshospitalet, Copenhagen, Denmark; ⁸Cell Differentiation Lab, Vrije Universiteit Brussel, Brussels, Belgium; ⁹Department of Surgery/Division of Orthopaedic Surgery, Children’s Hospital of Philadelphia, Philadelphia, Pennsylvania; and ¹⁰Cell and Developmental Biology, Vanderbilt University, Nashville, Tennessee



BACKGROUND & AIMS: Acinar-to-ductal metaplasia (ADM) is crucial in the development of pancreatic ductal adenocarcinoma. However, our understanding of the induction and resolution of ADM remains limited. We conducted comparative transcriptome analyses to identify conserved mechanisms of ADM in mouse and human. **METHODS:** We identified Sox4 among the top up-regulated genes. We validated the analysis by RNA in situ hybridization. We performed experiments in mice with acinar-specific deletion of Sox4 (*Ptf1a: CreER; Rosa26^{-LSL-YFP/SL-YFP}; Sox4^{fl/fl}*) with and without an activating mutation in *Kras* (*Kras^{LSL-G12D/+}*). Mice were given caerulein to induce pancreatitis. We performed phenotypic analysis by immunohistochemistry, tissue decellularization, and single-cell RNA sequencing. **RESULTS:** We demonstrated that Sox4 is reactivated in ADM and pancreatic intraepithelial neoplasias.

Contrary to findings in other tissues, Sox4 actually counteracts cellular dedifferentiation and helps maintain tissue homeostasis. Moreover, our investigations unveiled the indispensable role of Sox4 in the specification of mucin-producing cells and tuft-like cells from acinar cells. We identified Sox4-dependent non-cell-autonomous mechanisms regulating the stromal reaction during disease progression. Notably, Sox4-inferred targets are activated upon KRAS inactivation and tumor regression. **CONCLUSIONS:** Our results indicate that our transcriptome analysis can be used to investigate conserved mechanisms of tissue injury. We demonstrate that Sox4 restrains acinar dedifferentiation and is necessary for the specification of acinar-derived metaplastic cells in pancreatic injury and cancer initiation and is activated upon *Kras* ablation and tumor regression in mice. By uncovering novel potential strategies to

promote tissue homeostasis, our findings offer new avenues for preventing the development of pancreatic ductal adenocarcinoma.

Keywords: ADM; Plasticity; Tuft Cells; PDAC; Cancer Initiation.

Pancreatitis is a significant risk factor for the development of pancreatic ductal adenocarcinoma (PDAC).¹ Tissue damage induces acinar cells in the exocrine tissue to undergo acinar-to-ductal metaplasia (ADM), a process that involves the shutdown of a dedicated secretory program and the adoption of features of embryonic progenitor- and ductal-like cellular states.^{2,3} ADM enables quiescent mature cells to re-enter the cell cycle and recover from injury in epithelial tissues with a limited pool of somatic stem cells.⁴ Furthermore, ADM orchestrates tissue remodeling by recruiting immune cells, activating fibroblasts, and inducing changes in the extracellular matrix to aid in tissue repair. However, ADM also renders acinar cells vulnerable to neoplastic transformation.^{5,6} Somatic mutations in the Kristen rat sarcoma proto-oncogene (*Kras*) prevent the redifferentiation of acinar cells, leading to the formation of tumor precursor pancreatic intraepithelial neoplasia (PanINs) and potentially malignant transformation. A key aspect of PanINs is the induction of a stromal reaction and recruitment of immune cells into the tumor microenvironment supporting pancreatic tumorigenesis. These findings emphasize the importance of understanding the initiation and resolution of ADM and the interactions between epigenetic determinants of cell identity and genetic alterations in the early stages of PDAC.

The family of SRY-related high-mobility-group (HMG) box-containing transcription factors regulate cellular differentiation during the development and regeneration of multiple tissues.⁷ Specifically, *Sox4* and *Sox9* are widely expressed in pancreatic progenitors during development and are necessary for the specification of pancreatic lineages.^{8,9} Interestingly, *Sox4* is (re-)expressed in various epithelial tissues upon tissue injury and cancer development,¹⁰ such as prostate,¹¹ breast,¹² intestine¹³ and bladder,¹⁴ where it has been shown to promote stemness, proliferation, and tumor progression and metastasis. SOX transcription factor binding motifs are enriched in newly accessible chromatin domains during ADM and KRAS-induced PanIN formation.⁵ Although *Sox9* is a hallmark of ADM and necessary for PanIN formation,¹⁵ the function of *Sox4* in pancreas regeneration and cancer initiation has not been investigated.

Our study sheds light on the mechanisms underlying the adaptation of pancreatic acinar cells to tissue injury in both mouse and human models. The findings reveal the multifaceted role of *Sox4* in this context, wherein it promotes cellular differentiation, suppresses tumor formation, and regulates the remodeling of the tissue microenvironment in early neoplastic lesions. These insights enhance our understanding of the complex interplay between cellular differentiation, tissue microenvironment, pancreatic regeneration, and cancer.

WHAT YOU NEED TO KNOW

BACKGROUND AND CONTEXT

Acinar cell adaptation to tissue injury is linked to the onset of pancreatic ductal adenocarcinoma. However, our knowledge of the regulatory networks involved in damage resolution remains limited.

NEW FINDINGS

Upon tissue injury, the activation of a genetic program controlled by *Sox4* restricts further damage. *Sox4* regulates cellular differentiation and tissue remodeling through both cell-autonomous and nonautonomous mechanisms. Importantly, targets regulated by *Sox4* are activated during tumor regression after *Kras* depletion.

LIMITATIONS

Functional studies are required to determine *Sox4*'s role in ductal cells during tissue damage and inflammation.

CLINICAL RESEARCH RELEVANCE

Our work establishes an experimental platform to investigate the conserved mechanisms of acinar adaptation to injury, which has implications for pancreatitis recovery and pancreatic ductal adenocarcinoma initiation. Importantly, it offers valuable insights into pathways of tumor regression and escape, with potential implications for pancreatic ductal adenocarcinoma treatment, especially given recent progress in pharmacologic KRAS inhibition.

BASIC RESEARCH RELEVANCE

Pancreatic acinar cells exhibit remarkable plasticity, assuming alternative cell fates during tissue injury and inflammation, suggesting a collaborative effort in tissue recovery. Our *in vivo* findings emphasize the pivotal role of *Sox4* as a master regulator, driving tuft cell specification and gastric metaplasia in acinar plasticity. This research enhances our understanding of acinar cell healing, transdifferentiation, and the role of acinar plasticity in tissue remodeling and cancer initiation.


Methods

Human Tissue Samples

Ethical consent was given by the Committee of Medical Ethics–Universitair Ziekenhuis Brussels, and samples were obtained through the Central Biobank Universitair Ziekenhuis Brussel (17-183 and 20-466).

* Authors share co-first authorship.

Abbreviations used in this paper: ADM, acinar-to-ductal metaplasia; aSMA, alpha smooth muscle actin; iCAF, inflammatory cancer-associated fibroblast; ISH, in situ hybridization; HMG, high-mobility-group; KO, knockout; *Kras*, Kristen rat sarcoma proto-oncogene; myCAF, myofibroblast-like cancer-associated fibroblast; PanIN, pancreatic intraepithelial neoplasia; PDAC, pancreatic ductal adenocarcinoma; scRNAseq, single-cell RNA sequencing; WT, wild type; YFP, yellow fluorescent protein.

 Most current article

© 2024 The Author(s). Published by Elsevier Inc. on behalf of the AGA Institute. This is an open access article under the CC BY-NC-ND license (<http://creativecommons.org/licenses/by-nc-nd/4.0/>).

0016-5085

<https://doi.org/10.1053/j.gastro.2024.04.031>

Single-Cell RNA Sequencing Data Analysis

Raw base call (BCL) files generated by Illumina sequencers were demultiplexed into FASTQ files using the 10× Genomics Single-Cell Gene Expression Software Cell Ranger, version 7.2.0 (“mkfastq” pipeline, default parameters). The nf-core sc-rnaseq pipeline, version 2.4.1, was selected to perform a best-practice analysis pipeline for processing 10× Genomics single-cell RNA-sequencing (scRNAseq) data. 10× Genomics provided the reference genome sequenced: mouse reference (mm10-2020-A).

For in-depth analysis of major cell compartments (epithelial, fibroblasts, and macrophages), the initial dataset was subset and reclustered following the methodology in the Supplementary Methods. Clusters were annotated using canonical markers. Differential gene expression analysis was conducted using Seurat’s FindMarkers function (version 4.4.0) via the Wilcoxon test, leveraging the log-transformed expression matrix. Features with a log₂ fold change greater than 0.33 and an adjusted *P* value less than .05 were defined as differentially expressed genes.

Statistical Analysis

The statistical analysis of each experiment is described in the corresponding legend detailing the statistical tests used and sample sizes. High-throughput data, including RNA sequencing, were analyzed using specialized bioinformatics software and statistical packages. Differential expression analyses were adjusted for multiple testing using the false discovery rate. Differences between groups were assessed using parametric or nonparametric tests, as dictated by the normality of the data distribution and homogeneity of variances. For comparisons involving more than 2 groups, 1-way or 2-way analysis of variance was used, followed by post hoc tests for multiple comparisons where necessary. The level of significance was set at *P* < .05 for all tests.

Results

Sox4 Is Induced Upon Tissue Injury and Maintained in Pancreatic Intraepithelial Neoplasia

In this study, we aimed to identify the transcription factors that regulate acinar dedifferentiation. To accomplish this, we performed transcriptome analysis of both human exocrine explants in vitro, which mimics the acute damage response induced in pancreatic injury,¹⁶ and pancreas tissue from an experimental model of pancreatitis in mice induced by repeated injections of a cholecystokinin analog, caerulein (Figure 1A). We observed an overlap of pathways associated with tissue injury in both experimental models such as “KRAS_SIGNALING_UP,” “INFLAMMATORY_RESPONSE,” “INTERFERON_GAMMA_RESPONSE,” and “TNFA_SIGNALING_VIA_NFKB” (Figure 1B). We compared the datasets and found that 366 genes were commonly overexpressed. Among them, 22 genes encoding transcription factors were significantly up-regulated in the injury condition (Supplementary Table 1). They included the genes for the erythroblast transformation specific transcription factors ELF3 and ETS2, the HMG box-containing transcription factor SOX4, and the zinc finger-C2H2 transcription factors KLF7 and KLF5. We confirmed significant induction of the commonly

overexpressed metaplastic genes *KLF5* and *KRT19* and loss of the acinar differentiation markers *BHLHA15* (Supplementary Figure 1A). We validated the up-regulation of *Sox4* by single-molecule RNA in situ hybridization (ISH) (Supplementary Figure 1B). Supporting our transcriptome analysis, we found that *SOX4* expression was associated with chronic injury as well as PanINs and PDAC in human resected specimens (Figure 1C).

Next, we investigated the expression pattern of *Sox4* in an experimental mouse model of acinar regeneration and cancer initiation. We used the *Ptf1a: CreER; Kras^{LSL-G12D/+}; Rosa26^{-LSL-YFP/SL-YFP}* (KCY^{Acinar}) mice and subjected them to the same tissue injury and inflammation protocol. Upon tamoxifen injection in adult mice, KRAS^{G12D} protein is expressed specifically in *Ptf1a*-expressing acinar cells of the pancreas. Although KRAS^{G12D} is weakly oncogenic in acinar cells in homeostasis, it synergizes with signals activated after tissue injury and inflammation to generate PanINs.¹⁷ Our results showed that *Sox4* was highly up-regulated in acinar and ductal cells after tissue injury and, to a lesser extent, in stromal cells (Figure 1D and Supplementary Figure 1B). This expression pattern is consistent with the morphologic and molecular evidence of ADM, which is susceptible to neoplastic transformation driven by an activating mutation in *Kras*. Indeed, in contrast to control mice, where *Sox4* expression returned to basal levels, *Sox4* expression was maintained in all PanINs (Figure 1D). We validated our findings in normal pancreas, PanINs, and advanced PDACs in mouse (Supplementary Figure 2A–C).¹⁸ Of note, we found that *Sox4* was the top SOX transcription factor up-regulated in isolated acinar cells after injury, including *Sox11* and *Sox12* (which, together with *Sox4*, form the SOXC group within the SOX family), as well as *Sox9*, which was previously shown to regulate acinar plasticity (Supplementary Figure 2D).⁵ Furthermore, transcriptome and chromatin accessibility data confirmed *Sox4* up-regulation in both regeneration and cancer initiation in isolated acinar cells, in parallel with the loss of acinar markers (Supplementary Figure 3A and Supplementary Table 2).⁵ Notably, analysis of single-nucleus RNA sequencing from human chronic pancreatitis samples identified *SOX4* expression in tuft cells and in a subpopulation of *MUC5B⁺/KLF5⁺* cells reminiscent of the transitional cellular state observed in ADM (Supplementary Figure 3B).¹⁹ Taken together, these results demonstrate that *Sox4* is expressed in a transitional cellular state of acinar dedifferentiation that emerges after tissue injury and is maintained in precancerous lesions of PDAC.

Sox4 Expression Is Up-regulated After Acinar-to-Ductal Metaplasia

Next, we conducted a time course experiment using whole pancreas quantitative polymerase chain reaction and histopathologic analysis (Supplementary Figure 4A and B). After tissue injury and inflammation, the pancreas recovered after 14 days. Interestingly, we observed that the KRAS-induced transcription factors *Junb* and *Foxq1* were rapidly induced after injury, before the down-regulation of acinar markers and the up-regulation of ductal markers and

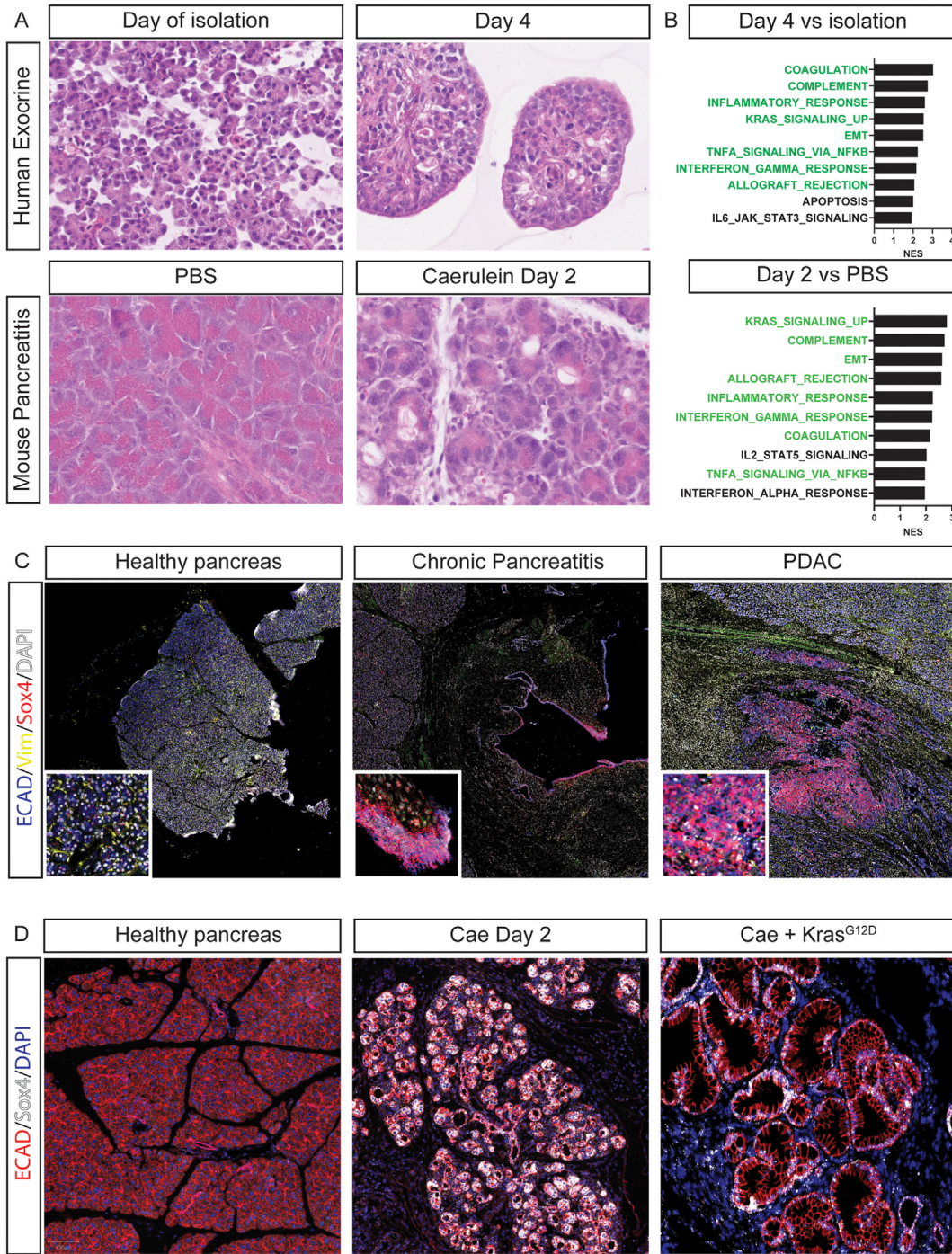


Figure 1. Sox4 expression is induced in ADM and ductal cells upon tissue injury. (A) We compared the gene expression profile of freshly isolated human exocrine pancreas the day of isolation and after 4 days in culture (top) with an experimental model of acute pancreatitis induced in mice with caerulein (bottom). Original magnification, 40×. (B) We observed a significant overlap (highlighted in green) of pathways in both models of acute damage. Gene set enrichment analysis of hallmarks was performed, and these were ranked according to normalized enrichment score (false discovery rate, <0.05). (C, D) We performed ISH and immunofluorescence analysis in human and mouse samples. SOX4 is up-regulated in E-cadherin⁺ ductal lesions with periductal fibrosis in chronic pancreatitis and PDAC (C). Sox4 is expressed in acinar and ductal cells upon induction of pancreatitis and PanINs in WT and KCY^{Acinar} mice (D). Images are representative of 3 resected specimens evaluated by an experienced pathologist. DAPI, 4',6-diamidino-2-phenylindole; NES, normalized enrichment score; PBS, phosphate-buffered saline.

before *Sox4* expression. The expression of *Sox4* was acutely up-regulated 2 days postinjection, coinciding with the up-regulation of markers of proliferation.

Sox4 Deletion Exacerbates Acinar Dedifferentiation Upon Tissue Injury

To investigate the potential role of *Sox4* in recovery from tissue injury, we deleted *Sox4* in mature acinar cells. Specifically, we generated *Ptf1a: CreER; Rosa26^{-LSL-YFP/LSL-YFP}; Sox4^{+/+}* (C*Sox4*^{WT}) and *Ptf1a: CreER; Rosa26^{-LSL-YFP/LSL-YFP}; Sox4^{fl/fl}* (C*Sox4*^{KO}) (Supplementary Figure 5A–C). ISH revealed an efficient deletion of the gene in most acinar-derived cells 2 days after inducing pancreatic injury, at the peak of *Sox4* expression (Figure 2A).

Because *Sox4* is not expressed in adult acinar cells, we did not observe any morphologic differences in the pancreas after *Sox4* deletion (Supplementary Figure 6A and B). However, histopathologic analysis 2 days after tissue injury, at the peak of *Sox4* expression, showed increased ADM, disturbed lobular architecture with increased fibrosis, and slightly distended and irregular luminal space in acinar-derived ductal-like structures in the *Sox4*-depleted pancreas compared to the wild-type (WT) control (Figure 2B). Additionally, instances of fibrotic pancreas were noted in C*Sox4*-knockout (KO) mice, a pathology not evident in C*Sox4*^{WT} littermates (Supplementary Figure 6C and D).

Next, we assessed the expression of markers associated with acinar differentiation and ADM in C*Sox4*^{WT} and C*Sox4*^{KO}. The loss of *Sox4* in acinar cells resulted in the up-regulation of *Klf5* and *Junb* in acinar-derived cells (Figure 2C), which have been shown to be expressed in the transitional cellular state primed to develop PanINs.⁶ Furthermore, we observed up-regulation of *Krt19*, *Cd44*, *Junb*, *Foxq1*, and *Sox9* and down-regulation of acinar-specific transcription factors *Bhlha15* (Figure 2D and Supplementary Figure 7A). These results suggest that *Sox4* restrains acinar metaplasia in response to damage rather than promotes it.

Sox4 Deletion Has Non-Cell-Autonomous Effects on the Stromal Compartment

To identify pathways regulated by *Sox4*, we performed RNA sequencing and gene set enrichment analysis on C*Sox4*^{WT} and C*Sox4*^{KO} pancreas 2 days after injury. We observed up-regulation of KRAS_SIGNALING_UP, TGF_BETA_SIGNALING, TNFA_SIGNALING_VIA_NFKB, and IL6_JAK_STAT3_SIGNALING in C*Sox4*^{KO} compared to C*Sox4*^{WT} mice (Figure 3A and Supplementary Table 3). These findings suggest that *Sox4* depletion induces a shift of acinar cells toward premalignancy in the absence of KRAS^{G12D}-activating mutations. Validating the gene expression signature, we observed increased phosphorylation of Stat3^{Tyr705} (Figure 3B) and increased TGFβ induced (TGFβI) and tenascin (TNC) deposition in the extracellular matrix of C*Sox4*^{KO} compared to C*Sox4*^{WT} (Figure 3C). Additionally, we observed a striking increase in the number of alpha smooth muscle actin (aSMA)-positive fibroblasts surrounding the pancreatic acinus in C*Sox4*^{KO} pancreas, which were mostly

confined to the periphery of ducts and vessels in C*Sox4*^{WT} mice (Figure 3D). Next, given that *Sox4* expression is concomitant with the up-regulation of Ki67 and that it has been shown to regulate proliferation in homeostasis and cancer in other tissues, we assessed cellular proliferation in the epithelium and aSMA⁺ fibroblasts. We observed a significant decrease in the number of proliferative acinar-derived cells and an increased proliferation of fibroblasts (Figure 3E). The increase in infiltration was specific to aSMA⁺ myofibroblast-like cancer-associated fibroblasts (myCAFs) (Figure 3F and Supplementary Figure 7B and E). Supporting an increase of aSMA⁺ fibroblasts, we observed up-regulation of extracellular matrix-associated proteins (eg, *COL12A1*, *COL11A1*, *LAMA3*, *COL8A1*, *FBN2*, *COL8A2*, *LAMC2*) (Supplementary Figure 7C). Notably, we did not observe an increase of apoptotic cells in C*Sox4*^{KO} compared to C*Sox4*^{WT}, indicating that the enhanced fibrotic response is not due to an increase of death cells (Supplementary Figure 8A). We did not observe changes in the total number of immune cells or macrophages (Supplementary Figure 8B). Overall, our transcriptome and histologic analysis demonstrate that after injury in the pancreas, *Sox4* regulates acinar proliferation, restrains acinar dedifferentiation, and suppresses STAT3 phosphorylation, the TGFβ pathway, and the activation of aSMA⁺ fibroblasts.

Sox4 Is Necessary for the Specification of Pancreatic Intraepithelial Neoplasia-Associated Cell Types

Our gene expression analysis demonstrates that *Sox4* expression is maintained in PanINs, associated with disease progression. To investigate the role of *Sox4* in the formation of PanIN lesions from acinar cells after tissue injury and KRAS mutations, we created mice that combined *Kras*^{G12D}-activating mutations with the deletion of *Sox4* in acinar cells. Specifically, we generated 2 groups of mice: *Ptf1a: CreER; Kras^{-LSL-G12D/+}; Rosa26^{-LSL-YFP/LSL-YFP}; Sox4^{+/+}* (KCS*Sox4*^{WT}) and *Ptf1a: CreER; Kras^{-LSL-G12D/+}; Rosa26^{-LSL-YFP/LSL-YFP}; Sox4^{fl/fl}* (KCS*Sox4*^{KO}). After 2 weeks of tamoxifen injection, we induced tissue injury and collected the pancreas after 21 days for further analysis. ISH validated *Sox4* recombination and showed a complete absence of *Sox4* transcript in a large number of acinar-derived cells in KCS*Sox4*^{KO} mice compared to expected up-regulation in the epithelial cells of KCS*Sox4*^{WT} mice, indicating efficient and specific recombination in acinar-derived cells (Supplementary Figure 9A).

We observed that the pancreas from KCS*Sox4*^{KO} mice had a significantly higher weight than the pancreas from KCS*Sox4*^{WT} mice (Supplementary Figure 9B). Histologic analysis revealed morphologic evidence of KRT19⁺ ductal-like lesions in both groups of mice, with disturbed lobular architecture, extensive fibrosis, and large irregular ductal structures lined by cells with large and hyperchromatic nuclei in KCS*Sox4*^{KO} and KCS*Sox4*^{WT} mice. Morphometric analysis of lesions showed decreased lesion area, while the lumen area is increased in the KCS*Sox4*^{KO} compared to KCS*Sox4*^{WT} mice (Figure 4A and Supplementary Figure 10).

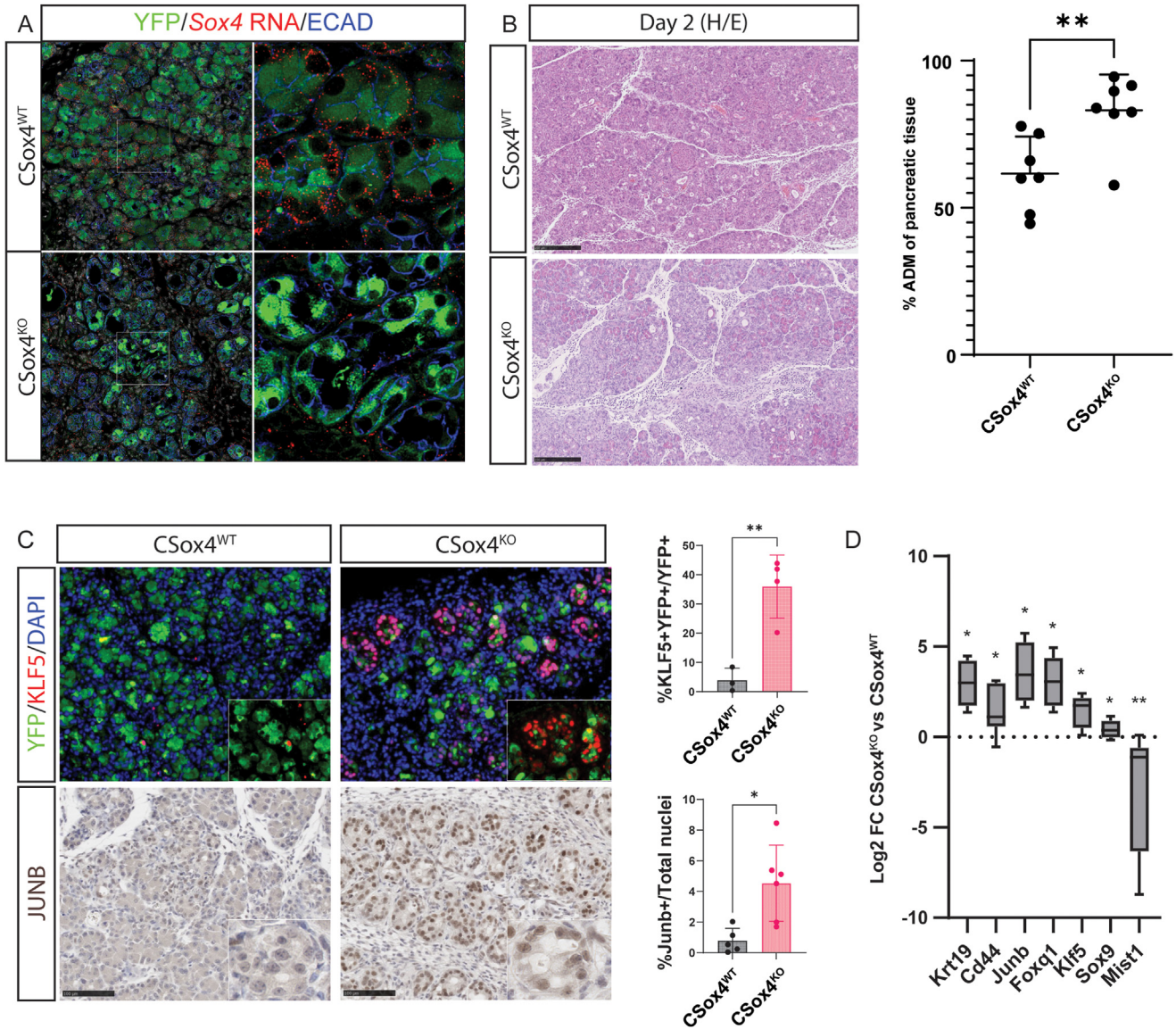


Figure 2. *Sox4* regulates the redifferentiation and proliferation of metaplastic acinar cells. (A) We confirmed the conditional KO of *Sox4* in acinar cells by ISH and immunofluorescence staining with epithelial markers. Most acinar-derived cells (YFP+) show loss of *Sox4* in CSox4^{KO} compared to CSox4^{WT}. Representative images from at least 3 mice are shown. Original magnification, 20× (left) and 80× (right). (B) Histopathologic analysis and ADM quantification of pancreatic tissue 2 days after induction of acute pancreatitis. We observed evidence of pancreatic injury in both groups. Representative images from at least 3 mice are shown. Scale bar, 250 μm. (C) We performed immunofluorescence and DAB staining for markers associated with acinar metaplasia. We observed focal areas of *Klf5* and *Junb* nuclear staining in CSox4^{KO} compared to CSox4^{WT}. We quantified *Klf5* and *Junb* nuclear staining as a percentage of acinar-derived YFP⁺ cells and total nuclei, respectively. Immunofluorescence original magnification, 20×. DAB scale bar, 100 μm. (D) We confirmed the histologic results by gene expression analysis of metaplastic and differentiation genes by quantitative polymerase chain reaction. Statistical tests performed in C and D are unpaired 2-tailed Student *t* test comparing KO with WT samples. *P* value is indicated on the graph, or **P* < .05, ***P* < .01. All experiments were performed in at least 3 mice. DAB, 3,3'-diaminobenzidine tetra hydrochloride; DAPI, 4',6-diamidino-2-phenylindole; H/E, hematoxylin and eosin.

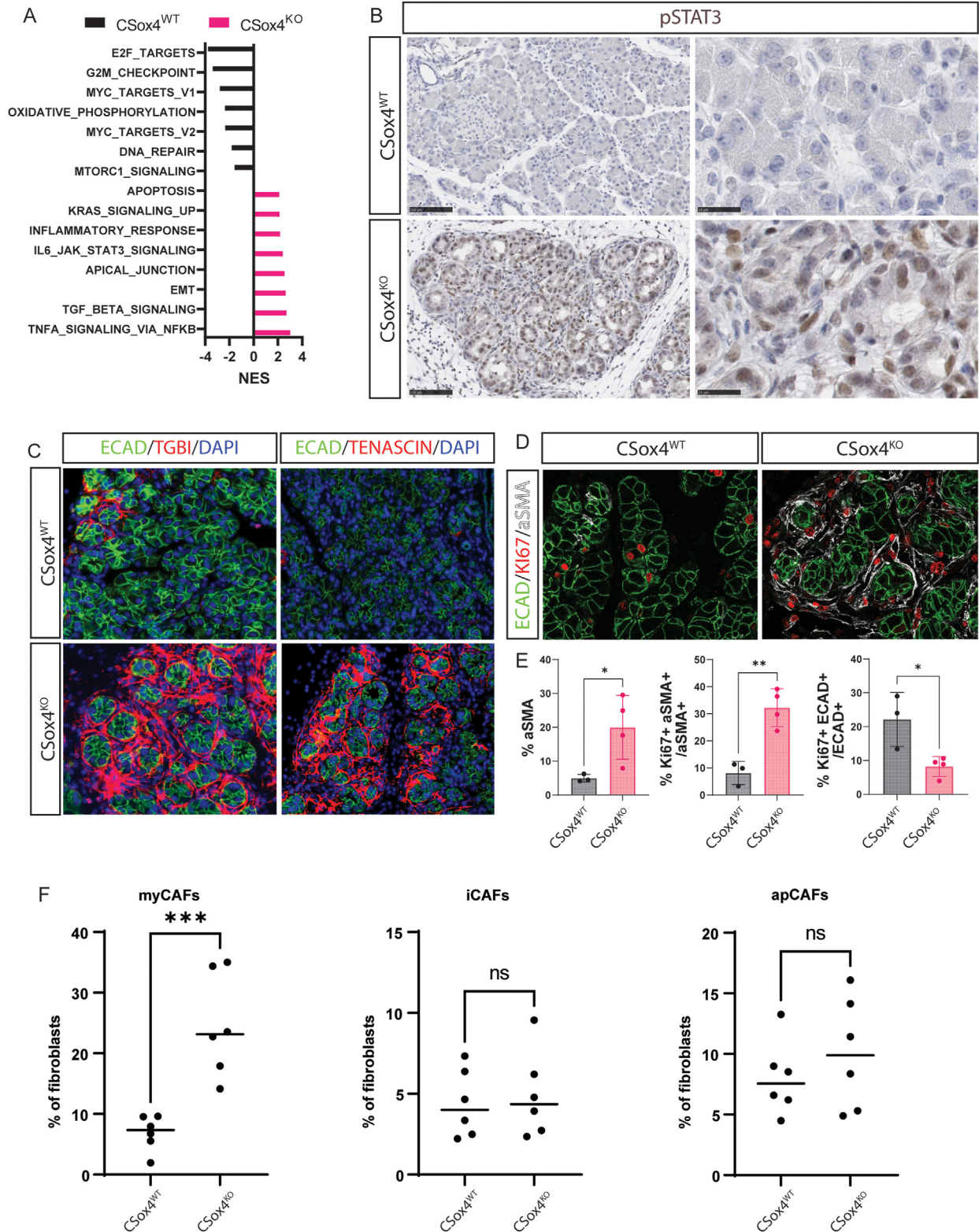
We observed an almost complete depletion of the mucinous-filled cytoplasm of the epithelial cells in KCSox4^{KO} mice compared to KCSox4^{WT} mice (Figure 4A). Supporting these observations, we determined that *Sox4* is specifically expressed at the branching point of tuft cell and enteroendocrine specification in a mouse model of chronic pancreatitis (Supplementary Figure 11A). Furthermore, gene regulatory network analysis of scRNAseq revealed that

Sox4 regulates *Pou2f3* and *Neurog3*, master regulators of Tuft cells and enteroendocrine cells (Supplementary Table 4). It is noteworthy that occasional columnar epithelium cells that express *Sox4* could be observed within the same lesion. These cells escape Cre-mediated recombination, indicating that *Sox4*-dependent mucinous specification is a cell-autonomous process (Supplementary Figure 11B). This observation highlights the importance of *Sox4* in the

transdifferentiation of acinar cells in the development of PanINs.

Next, we performed immunohistochemistry and immunofluorescence analysis of POU2F3, DCLK1, and MUC5AC, markers for tuft-like and pit-like cells, respectively, in the

pancreas of KCSox4^{WT} and KCSox4^{KO} mice 21 days after the induction of tissue injury (Figure 4B). In KCSox4^{WT} mice, DCLK1-positive tuft-like cells were found to be juxtaposed to MUC5AC-positive pit-like cells, and both types of cells were found to colocalize with yellow fluorescent protein



(YFP) (Supplementary Figure 11B), indicating their lineage relationship with acinar cells. In contrast, there was a near depletion of pit-like and tuft-like cells in KCSox4^{KO} mice, suggesting that *Sox4* is necessary for the specification of subpopulations of cell lineages derived from acinar cells and induced after tissue injury and *Kras*^{G12D} activation.

Next, we performed bulk RNA sequencing analysis in whole pancreas extracted from KCSox4^{WT} and KCSox4^{KO} mice to investigate the role of *Sox4* in acinar plasticity in PanIN lesions (Supplementary Table 5). Despite losing the specification of acinar-derived lineages, *Sox4* did not affect the expression of the transcription factor–encoding genes *Junb* and *Onecut2* and ductal markers *Krt19* and *Krt7* (Supplementary Table 5). We performed gene ontology analysis of differentially expressed genes in KCSox4^{KO} mice compared to KCSox4^{WT} and observed up-regulation of pathways associated with the KRAS signaling pathway and immune function, among others (Figure 4C). These data suggest a possible role of *Sox4* in restraining disease progression and remodeling of the microenvironment in PanIN lesions.

Confirming previous histopathologic analysis, we observed a significant down-regulation of *Muc5ac* and *Dclk1* gene expression in KCSox4^{KO} mice compared to KCSox4^{WT} mice. Additionally, we observed an overall down-regulation of markers of chief-like cells (*Pgc*), pit-like cells (*Cldn18*, *Muc5ac*, *Tff1*, *Gkn1/2*), tuft-like cells (*Pou2f3*, *Dclk*), and enteroendocrine cell progenitors (*Neurog3*) in KCSox4^{KO} mice (Figure 4D and E and Supplementary Table 5),^{20,21} indicating that *Sox4* is necessary for acinar plasticity in preinvasive lesions. Notably, tuft cells and pit-like cells have been shown to restrain the growth of PanINs.²² These data suggest that *Sox4*-dependent acinar plasticity represents a protective mechanism in the progression of PDAC.

Sox4 Exerts Prohomeostatic Functions Through Cell-Autonomous and Non-Cell-Autonomous Processes in Preinvasive Lesions

PDAC initiation involves extensive tissue remodeling and the generation of an immunosuppressive environment, starting from the PanIN stage.²³ We aimed to determine if

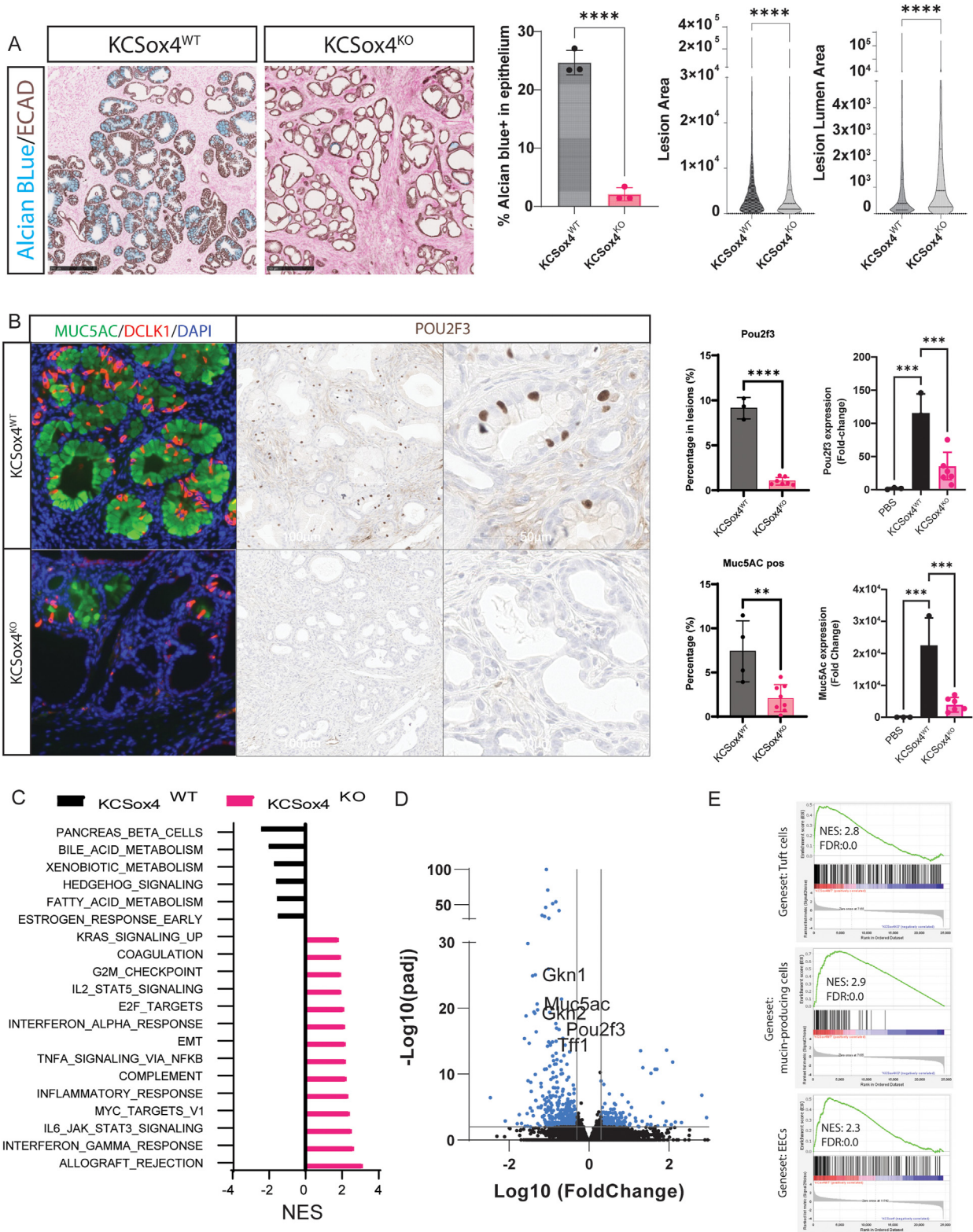
the loss of *Sox4* is associated with changes in the tumor microenvironment. We noted that the pancreas in KCSox4^{KO} mice was stiffer, indicative of an exacerbated stromal reaction. To further investigate collagen deposition in the extracellular matrix, we performed Fast Green and Sirius Red staining, in addition to pancreas decellularization, followed by staining for collagen XII. Fast Green and Sirius Red staining and analysis of decellularized tissue from KCSox4^{KO} mice revealed increased collagen XII deposition around lesions and a visible linearization of collagen fibers, suggesting a desmoplastic-like reaction in these areas (Figure 5A and Supplementary Figure 12). Subsequently, we performed immunohistochemical analyses for CD45 and F4/80 in both KCSox4^{KO} and KCSox4^{WT} littermates, with and without caerulein-induced tissue damage. We observed a significant increase in infiltrating immune cells in both groups after the induction of tissue injury (Figure 5B and C). Interestingly, despite an equal number of macrophages, there was a notable reduction in the total number of CD45⁺ immune cells in KCSox4^{KO} mice compared to KCSox4^{WT} controls. These data suggest that the loss of *Sox4* may contribute to the development of a desmoplastic and immune-depleted environment, which is associated with disease progression.

To investigate changes in cell populations due to *Sox4* depletion in the epithelium, we performed scRNAseq on pancreatic tissue isolated from CSox4^{KO} and CSox4^{WT} mice, 2 days after tissue injury induction and in a phosphate-buffered saline control group. Additionally, we profiled single cells from KCSox4^{KO} mice both 2 days and 21 days after tissue injury to assess *Sox4*'s role in disease progression. We used uniform manifold approximation and projection to visualize epithelial and nonepithelial cells, categorizing them based on established lineage markers (Figure 6A). Our findings indicate that *Sox4* loss leads to an exacerbated epithelial response to injury, marked by increased expression of tissue damage and disease progression markers such as *Cldn4*, *Mmp7*, *Krt19*, *Cxcl16*, and *Ly6a*, alongside a decrease in differentiation markers like *Bhlha15*, *Cpa1*, *Cpa2*, *Cela1*, and *Rbpjl* in CSox4^{KO} epithelial cells compared to CSox4^{WT} (Figure 6B and Supplementary Table 6). To further understand the state of epithelial cells in CSox4^{KO} mice, we analyzed the expression of

Figure 3. *Sox4* prevents the activation of signaling pathways associated with tissue damage. (A) We performed gene expression analysis (gene set enrichment analysis) in whole pancreas extracted from CSox4^{WT} and CSox4^{KO} 2 days after induction of pancreatitis. Gene sets are ordered by normalized enrichment score. False discovery rate, <0.05. (B) We performed DAB staining for phosphorylated (p) STAT3^{Tyr705}. We observed an increase in pSTAT3^{Tyr705} in the nucleus of acinar and surrounding stromal cells in CSox4^{KO} compared to CSox4^{WT}. Scale bar, 100 μm. (C) We performed immunofluorescence analysis for TGFB induced and tenascin. We observed an increased deposition of both proteins in the extracellular space surrounding the metaplastic acinus in CSox4^{KO} compared to Csox4^{WT}. Original magnification, 40×. (D) We performed immunofluorescence analysis to determine the proliferation index of compartment-specific cell types using Ki67. Loss of *Sox4* results in decreased proliferation of metaplastic acinar cells and increased proliferation of aSMA⁺ fibroblasts. Original magnification, 40×. (E) Quantification of respective staining in CSox4^{WT} (n = 3) and CSox4^{KO} (n = 4) animals. (F) Percentage of myCAFs (aSMA⁺), apCAFs (aSMA⁻Ly6C⁺MHCII⁺), and iCAFs (aSMA⁻Ly6C⁺MHCII⁻) of total fibroblasts (CD45⁻CD31⁻CD326⁻Podoplanin⁺) assessed by flow cytometry. For more information, refer to Supplementary Figures 7B and 8. Unpaired 2-tailed Student *t* test comparing CSox4^{KO} with CSox4^{WT} samples. **P* < .05, ****P* < .01. All experiments were performed in at least 3 mice. Data are represented as mean ± standard deviation. apCAF, antigen-presenting cancer-associated fibroblast; DAB, 3,3'-diaminobenzidine tetra hydrochloride; DAPI, 4',6-diamidino-2-phenylindole; NES, normalized enrichment score; ns, not significant.

differentially expressed genes and compared them with the expression profiles of epithelial cells at various stages of injury-induced metaplasia and neoplasia. This comparison revealed a pronounced shift toward advanced metaplasia and neoplasia in *CSox4*^{KO} mice relative to *CSox4*^{WT} mice (Supplementary Figure 13).

Next, we noted an increase in the number of ACTA2⁺ myCAFs after tissue injury and inflammation induction in both *CSox4*^{WT} and *CSox4*^{KO} mice treated with caerulein, relative to the PBS control (Figure 6C–E). The abundance of myCAFs was significantly higher in *CSox4*^{KO} mice than in *CSox4*^{WT} littermates, with a continuous increase observed



as disease progressed in KCSox4^{KO} mice. These findings corroborate our earlier immunofluorescence and flow cytometry analyses, which indicated that *Sox4* deletion leads to the activation and proliferation of myCAFs in CSox4^{KO} compared to CSox4^{WT}. Intriguingly, our data demonstrate that although *Sox4* loss induces transcriptional alterations associated with advanced metaplasia and neoplasia only in a subset of epithelial cells, these changes significantly influence the remodeling of the tissue microenvironment.

Our previous analysis did not show differences in the immune component of the preneoplastic tissue microenvironment despite a significant reduction in the total amount of immune cells as the disease progresses. However, analysis of the scRNAseq uncovers an unappreciated heterogeneity within the macrophage's population in the CSox4^{WT} and CSox4^{KO} mice. Most notably, there was a notable increase in the proportion of macrophages expressing arginase 1 (*Arg1*) in CSox4^{KO} compared to CSox4^{WT} mice, and the number increases in KCSox4^{KO} mice. Recent studies have shown that *Arg1* marks a population of polarized macrophages driven by KRAS mutation in the epithelium only present in a preneoplastic TME and contributes to an immunosuppressive environment.²⁴ Interestingly, we observed a significant increase in Arg1⁺ macrophages in the absence of KRAS^{G12D} mutation, suggesting that *Sox4* restrains KRAS signaling in the epithelium. Furthermore, we observed an increase in *Tgfb1* expression, which is restricted to the Arg1⁺ population of macrophages. These data demonstrate that *Sox4* regulates the polarization of macrophages and suggest that the enhanced activation of myCAFs may be mediated by the indirect secretion of *Tgfb1* by Arg1⁺ macrophages in the CSox4^{KO} mice compared to CSox4^{WT} mice.

Our data reveal that *Sox4* deletion accelerates pancreatic disease, which is consistent with the up-regulation of KRAS_SIGNALING_UP. As such, *Sox4* targets may serve as potential regulators of tumor regression. To investigate this hypothesis, we compared the inferred target genes of *Sox4* with the transcriptional profile of PDAC tumors where KRAS expression has been genetically or pharmacologically inhibited.^{25,26} Interestingly, the extinction of KRAS resulted in tumor regression and the up-regulation of *Sox4* and genes that overlap with our set of inferred targets (Supplementary

Figure 14A–C). This observation suggests a potential connection between *Sox4* targets and the genetic/pharmacologic inhibition of KRAS. Further exploration of this overlap could provide valuable insights into the mechanisms underlying pancreatic healing and tumor regression.

Discussion

Tissue injury plays a crucial role in the initiation of PDAC in both mouse and human. Although recent studies have provided insights into the regulatory networks driving the adaptation of acinar cells to injury,^{5,6,27} the regulatory networks involved during the resolution of damage remain poorly understood. In our study, we investigated the role of *Sox4*, a transcription factor that is newly expressed in acinar cells after injury. Our findings revealed that deletion of *Sox4* resulted in prolonged expression of proteins in the AP-1 complex, increased expression of metaplastic genes, and reduced epithelial proliferation. Furthermore, *Sox4* is necessary for the specification of acinar-derived cell types in PanIN lesions. The loss of *Sox4* also influenced the composition of the tissue microenvironment, characterized by increased deposition of TGFβ ligands and heightened activation of myofibroblasts and polarization of macrophages, suggesting a proinflammatory phenotype. Therefore, our data strongly indicate that *Sox4* contributes to the resolution of acinar cell injury-induced pancreatitis.

Sox4 is widely accepted as an oncogene due to its frequent up-regulation during disease progression.²⁸ Our expression analysis of both mouse and human samples supports this notion because we observed a positive correlation between *Sox4* expression and PDAC progression. Interestingly, our genetic functional analysis demonstrated that *Sox4* loss actually exacerbates tissue damage and cellular dedifferentiation in pancreatitis and PanINs, hallmarks of cancer risk and poor prognosis. Recent studies have demonstrated that acinar cells have the remarkable capacity to adopt alternative cellular states, suggesting that there is a division of labor among specialized cells in the resolution or adaptation to injury.^{5,20,21,29,30} Our study demonstrates that *Sox4* is essential for the specification of acinar-derived cell lineages in precursor lesions.

Figure 4. *Sox4* is necessary for the specification of cell lineages in PanINs. (A) We performed histopathologic analysis of pancreatic tissue 21 days after induction of acute pancreatitis in KCSox4^{WT} and KCSox4^{KO} mice. We observed numerous lesions occurring in both phenotypes that were slightly smaller and devoid of mucin-producing cells as determined by alcian blue staining in the KCSox4^{KO} pancreas compared to KCSox4^{WT}. Scale bar, 250 μm. (B) We performed immunofluorescence analysis with markers of tuft (DCLK1) and mucinous (MUC5AC) cells and DAB of tuft cell marker POU2F3. Both cell types were largely absent in lesions from KCSox4^{KO} pancreas compared to KCSox4^{WT}. We quantified the number of positive tuft and mucinous cells and validated the results by gene expression analysis. Data are represented as mean ± standard deviation. Immunofluorescence original magnification, 40×. DAB original magnification, 20× (left) and 80× (right). (C–E) We performed RNA sequencing in KCSox4^{WT} and KCSox4^{KO} 21 days after induced injury. Gene set enrichment analysis shows enrichment of immune system processes, including adaptive immune responses in preinvasive lesions of KCSox4^{KO} pancreas compared to KCSox4^{WT} (C). Volcano plot depicting the expression of markers of cell lineages identified in PanINs (D). Gene set enrichment analysis using a gene set for tuft cells, mucin-producing cells, and EECs obtained in Schlesinger et al.²¹ (E). Unpaired 2-tailed Student *t* test comparing KO and PBS with WT samples. Experiments performed in at least 3 mice. **P* < .05, ***P* < .01, ****P* < .001, *****P* < .0001. DAB, 3,3'-diaminobenzidine tetra hydrochloride; EEC, enteroendocrine cell; FDR, false discovery rate; NES, normalized enrichment score; PBS, phosphate-buffered saline.

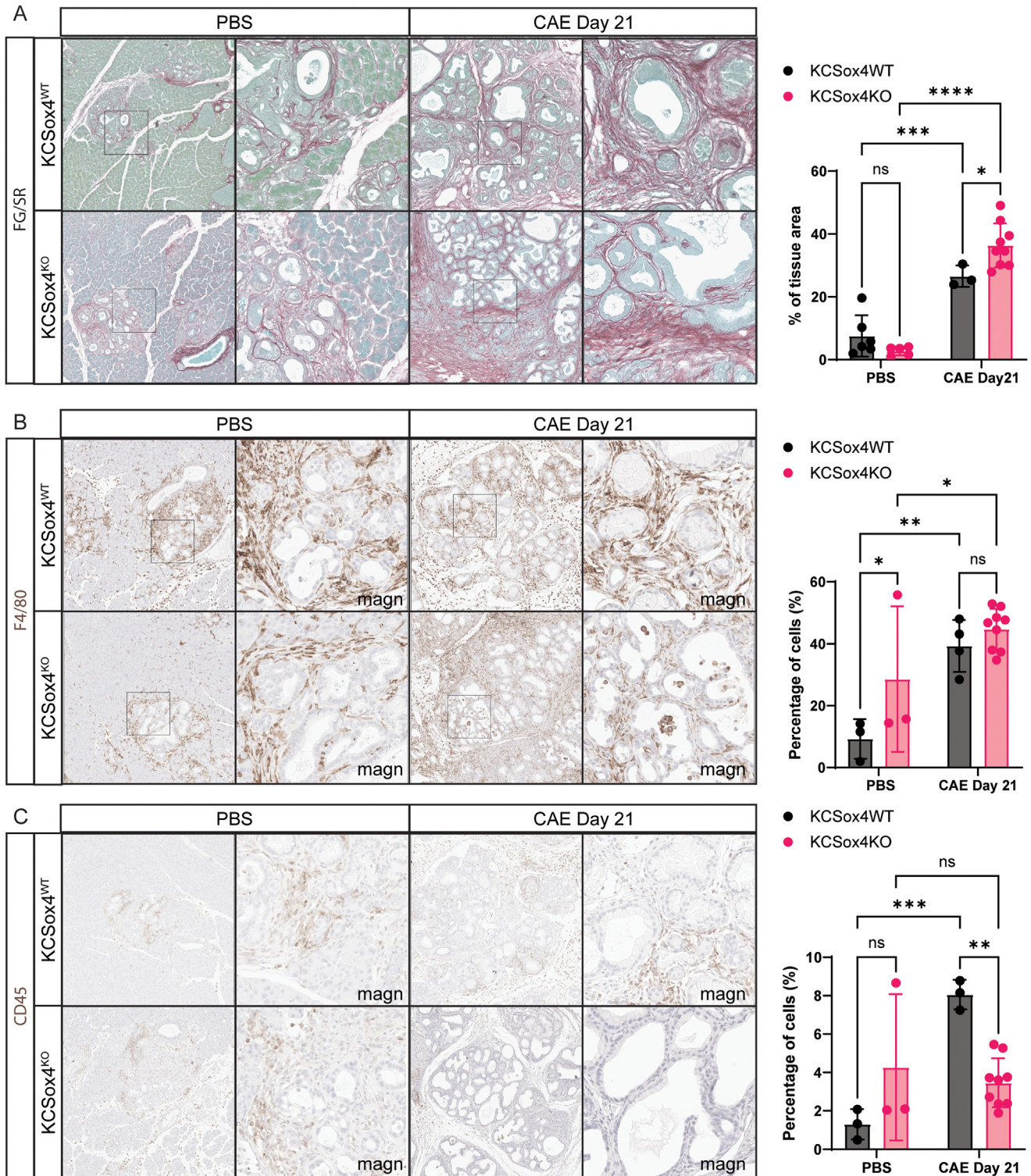
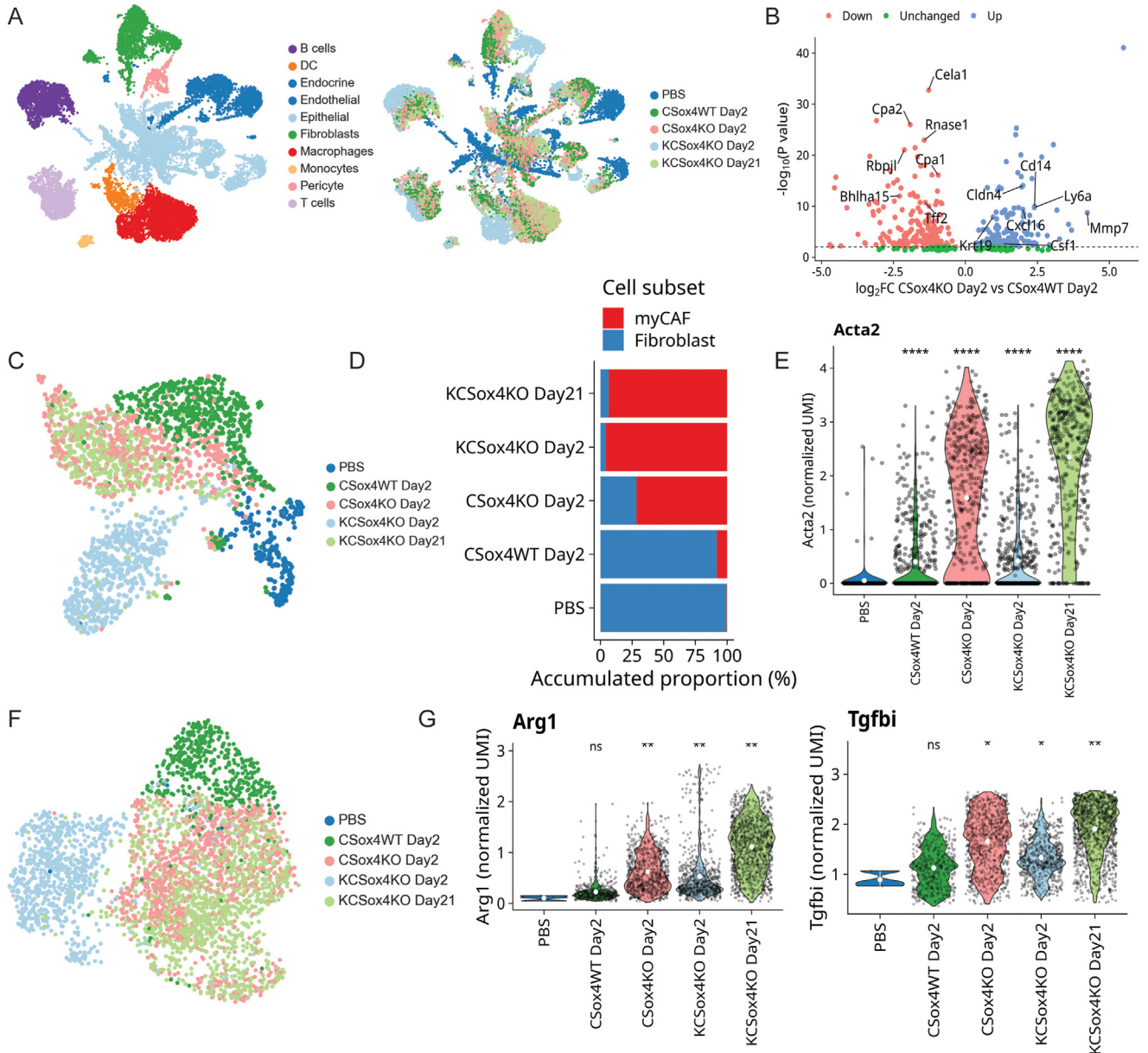


Figure 5. Sox4 regulates tissue homeostasis through autonomous and non-cell-autonomous mechanisms. We investigated changes in the microenvironment 21 days after caerulein-induced injury in KCSox4^{WT} and KCSox4^{KO} mice. PBS-injected animals were used as controls. (A) We investigated the collagen deposition in the extracellular matrix using Fast Green and Sirius Red staining. We observed higher collagen deposition in injury-induced tissues, exacerbated in KCSox4^{KO} mice. (B) We performed DAB against the macrophage marker F4/80. We observed higher macrophage infiltration in caerulein-injected tissues compared to PBS. Sox4 deletion in acinar cells did not lead to significant changes in macrophage infiltration. (C) We performed DAB analysis with a marker of immune cells. Caerulein-induced injury resulted in higher tissue infiltration in KCSox4^{WT} but not in KCSox4^{KO} mice. Statistical tests performed are 2-way analysis of variance with multiple comparisons. * $P < .05$, ** $P < .01$, *** $P < .001$, **** $P < .0001$. Data are represented as mean \pm standard deviation. All experiments were performed in at least 3 mice. Original magnification, 10 \times and 80 \times . CAE, caerulein; DAB, 3,3'-diaminobenzidine tetra hydrochloride; FG/SR, Fast Green and Sirius Red; magn, magnification; ns, not significant; PBS, phosphate-buffered saline.



PANCREAS

Figure 6. *Sox4* deletion exacerbates pancreatic injury. (A) UMAP includes all cells from 5 experiments. Data were produced from 5 samples, with 3 mice per sample. Cell types were determined based on the expression level of representative markers. (B) Differentially expressed genes in epithelial compartment: volcano plot showing genes significantly differentially expressed (P value $< .05$) between $CSox4^{KO}$ and $CSox4^{WT}$ cells. Up-regulated genes in $CSox4^{KO}$ (\log_2 fold change > 0) are shown in blue, and down-regulated genes (\log_2 fold change < 0) are in red. Selected gene names are highlighted. P values were adjusted for false discovery rate using the Benjamini-Hochberg correction. (C) Fibroblasts: UMAP includes all fibroblasts across 5 experiments. (D) Fibroblast subpopulations: bar plot showing the distribution of fibroblast subpopulations across different samples. (E) *Acta2* expression in fibroblasts: violin plot showing the expression level of *Acta2* by fibroblasts in different samples. Significant differences between groups were assessed using the Wilcoxon test. $*P < .05$, $**P < .01$, $***P < .001$. (F) Macrophages: UMAP includes all macrophages across 5 experiments. (G) Violin plot showing the expression level of *Arg1* and *Tgfb* by macrophages in different samples. Significant differences were assessed using the Wilcoxon test. $*P < .05$, $**P < .01$, $***P < .001$. DC, dendritic cell; NES, normalized enrichment score; ns, not significant; PBS, phosphate-buffered saline; UMAP, uniform manifold approximation and projection.

Although acinar-derived metaplastic cells possess tumor-forming capabilities,^{31,32} our data show that they functionally prevent the generation of a desmoplastic and anti-inflammatory tumor microenvironment. These results suggest that the cellular heterogeneity found in PanINs may restrain malignant transformation through nonautonomous mechanisms. Interestingly, this possibility has been proposed to explain the high prevalence of PanINs that do not progress to PDAC in the human disease.³³ Among the diverse population of acinar-derived cell types, tuft cells play a crucial role in restraining disease progression by promoting tissue homeostasis in the pancreas.^{34–36} Both *Sox4* KO and tuft cell depletion result in increased activation of fibroblasts, enhanced fibrosis, and polarization of myeloid-derived immune cells, all of which contribute to accelerated disease progression.³⁰ Therefore, our data indicate that the prohomeostatic function of *Sox4* may be mediated at least in part by the differentiation of tuft cells.³⁴ It is worth noticing that tuft cells have been shown to coordinate goblet hyperplasia in the gastrointestinal tract and epithelial airways in an anti-helminth immunity response.³⁷ We observed a drastic reduction of mucin-producing cells in *KCSox4*^{KO}, suggesting that a similar process may take place in the pancreas in response to sustained injury induced by *Kras* activation. This implies the existence of a conserved program of tissue regeneration that is shared among various endoderm-derived tissues.

Our scRNAseq analysis revealed that *Sox4* depletion leads to an increased population of *Arg1*⁺ macrophages. Previous research has indicated that *Arg1* expression is promoted by oncogenic *Kras* expression in epithelial cells during the early stages of pancreatic cancer.²⁴ Furthermore, *Arg1*⁺ polarized macrophages are known to inhibit T-cell expansion and contribute to an immunosuppressive microenvironment.²⁴ Interestingly, our study also found that *Arg1*⁺ cells are a primary source of *Tgfb1* expression, suggesting their crucial role in the activation of myCAF^s after *Sox4* deletion. Consequently, our findings imply that *Sox4* plays a dual role in limiting *Kras* signaling within the epithelium and in hindering disease progression through both cell-autonomous and nonautonomous mechanisms.

The results suggest that *Sox4* regulates a genetic program linked to the maintenance and restoration of tissue homeostasis and tumor regression upon the extinction of *KRAS*^{G12D}. Importantly, tumors capable of relapsing after the genetic ablation of *KRAS*^{G12D} exhibit molecular characteristics similar to those observed in the conditional deletion of *Sox4*. These characteristics include the phosphorylation of STAT3 at the Tyr705 residue and the induction of epithelial-mesenchymal transition.³⁸ This finding suggests a potential interplay between *Sox4* and *KRAS* signaling in the context of pancreatic tissue regeneration and cancer initiation that is bypassed in relapses. The emergence of targeting strategies for *KRAS*-driven cancers has opened up new opportunities for therapeutic interventions that hold promise for achieving a cure. However, to prevent drug resistance and tumor relapse, it is crucial to gain a better understanding of the underlying mechanisms involved in the healing process.

Our study has certain limitations because we focused solely on the role of *Sox4* in acinar-derived cells as a potential cancer cell of origin in PDAC. However, previous studies have identified both ductal and acinar cells as potential cells of origin for PDAC, and ductal cells have been shown to play a critical role in paracrine signaling, immune cell recruitment, and tissue remodeling,³⁹ processes that we found to be regulated by *Sox4* in acinar cells. Importantly, recent methylome analysis of human PanINs as well as acinar and ductal cells suggests acinar cells as the cell of origin in PDAC, through an intermediate cellular state that resembles acinar and ductal cells,⁴⁰ underscoring the relevance of understanding acinar metaplasia and acinar-specific modulation of the tissue environment and disease progression. Additionally, no changes were detected in the inflammatory cancer-associated fibroblast (iCAF) population, possibly due to the analysis occurring at early time-points. It has been observed that MyCAF/iCAF populations tend to segregate later in disease progression.⁴¹ Consequently, future research should focus on investigating *Sox4*'s role in ductal cells, assessing the impact of *Sox4* deletion on the differentiation of epithelial cancer cells, and examining fibroblast heterogeneity in both primary and metastatic tumors using mouse models of advanced disease.

Our findings in human models of acute damage and transcriptional profiling of precursor lesions indicate that the expression pattern and function of *Sox4* is conserved across species. This opens an opportunity to investigate strategies aimed at resolving tissue damage associated with human pancreatic pathologies.

Supplementary Material

Note: To access the supplementary material accompanying this article, visit the online version of *Gastroenterology* at www.gastrojournal.org, and at <https://doi.org/10.1053/j.gastro.2024.04.031>.

References

1. Gandhi S, de la Fuente J, Murad MH, et al. Chronic pancreatitis is a risk factor for pancreatic cancer, and incidence increases with duration of disease: a systematic review and meta-analysis. *Clin Transl Gastroenterol* 2022;13(3):e00463.
2. Jensen JN, Cameron E, Garay MV, et al. Recapitulation of elements of embryonic development in adult mouse pancreatic regeneration. *Gastroenterology* 2005; 128:728–741.
3. Pinho AV, Rooman I, Real FX. p53-dependent regulation of growth, epithelial-mesenchymal transition and stemness in normal pancreatic epithelial cells. *Cell Cycle* 2011;10:1312–1321.
4. Brown JW, Cho CJ, Mills JC. Paligenosis: cellular remodeling during tissue repair. *Annu Rev Physiol* 2022; 84:461–483.
5. Alonso-Curbelo D, Ho YJ, Burdziak C, et al. A gene-environment-induced epigenetic program initiates tumorigenesis. *Nature* 2021;590(7847):642–648.

6. Li Y, He Y, Peng J, et al. Mutant *Kras* co-opts a proto-oncogenic enhancer network in inflammation-induced metaplastic progenitor cells to initiate pancreatic cancer. *Nature Cancer* 2021;2:49–65.
7. Gracz AD, Magness ST. *Sry*-box (*Sox*) transcription factors in gastrointestinal physiology and disease. *Am J Physiol Gastrointest Liver Physiol* 2011;300:G503–G515.
8. Xu EE, Sasaki S, Speckmann T, et al. *SOX4* allows facultative β -cell proliferation through repression of *Cdkn1a*. *Diabetes* 2017;66:2213–2219.
9. Seymour PA, Shih HP, Patel NA, et al. A *Sox9*/*Fgf* feed-forward loop maintains pancreatic organ identity. *Development* 2012;139:3363–3372.
10. Vervoort SJ, van Boxtel R, Coffey PJ. The role of *SRY*-related HMG box transcription factor 4 (*SOX4*) in tumorigenesis and metastasis: friend or foe? *Oncogene* 2013;32:3397–3409.
11. Schärer CD, McCabe CD, Ali-Sayed M, et al. Genome-wide promoter analysis of the *SOX4* transcriptional network in prostate cancer cells. *Cancer Res* 2009;69:709–717.
12. Zhang J, Liang Q, Lei Y, et al. *SOX4* induces epithelial-mesenchymal transition and contributes to breast cancer progression. *Cancer Res* 2012;72:4597–4608.
13. Gracz AD, Samsa LA, Fordham MJ, et al. *Sox4* promotes *Atoh1*-independent intestinal secretory differentiation toward tuft and enteroendocrine fates. *Gastroenterology* 2018;155:1508–1523.
14. Aaboe M, Birkenkamp-Demtroder K, Wiuf C, et al. *SOX4* expression in bladder carcinoma: clinical aspects and in vitro functional characterization. *Cancer Res* 2006;66:3434–3442.
15. Kopp JL, von Figura G, Mayes E, et al. Identification of *Sox9*-dependent acinar-to-ductal reprogramming as the principal mechanism for initiation of pancreatic ductal adenocarcinoma. *Cancer Cell* 2012;22:737–750.
16. Baldan J, Houbracken I, Rooman I, et al. Adult human pancreatic acinar cells dedifferentiate into an embryonic progenitor-like state in 3D suspension culture. *Sci Rep* 2019;9(1):4040.
17. Hingorani SR, Petricoin EF, Maitra A, et al. Preinvasive and invasive ductal pancreatic cancer and its early detection in the mouse. *Cancer Cell* 2003;4:437–450.
18. Ling J, Kang Y, Zhao R, et al. *Kras*^{G12D}-induced *IKK2*/ β /*NF- κ B* activation by *IL-1 α* and *p62* feedforward loops is required for development of pancreatic ductal adenocarcinoma. *Cancer Cell* 2012;21:105–120.
19. Tosti L, Hang Y, Debnath O, et al. Single-nucleus and in situ RNA-sequencing reveal cell topographies in the human pancreas. *Gastroenterology* 2021;160:1330–1344.
20. Schlesinger Y, Yosefov-Levi O, Kolodkin-Gal D, et al. Single-cell transcriptomes of pancreatic preinvasive lesions and cancer reveal acinar metaplastic cells' heterogeneity. *Nat Commun* 2020;11(1):4516.
21. Ma Z, Lytle NK, Chen B, et al. Single-cell transcriptomics reveals a conserved metaplasia program in pancreatic injury. *Gastroenterology* 2022;162:604–620.
22. Steiner S, Seleznik GM, Reding T, et al. De novo expression of gastrokines in pancreatic precursor lesions impede the development of pancreatic cancer. *Oncogene* 2022;41:1507–1517.
23. Lee JW, Komar CA, Bengsch F, et al. Genetically engineered mouse models of pancreatic cancer: the KPC model (*LSL-Kras*^{G12D/+}; *LSL-Trp53*^{R172H/+}; *Pdx-1-Cre*), its variants, and their application in immuno-oncology drug discovery. *Curr Protoc Pharmacol* 2016;73:14.39.1–14.39.20.
24. Menjivar RE, Nwosu ZC, Du W, et al. Arginase 1 is a key driver of immune suppression in pancreatic cancer. *Elife* 2023;12:e80721.
25. Ying H, Kimmelman AC, Lyssiotis CA, et al. Oncogenic *Kras* maintains pancreatic tumors through regulation of anabolic glucose metabolism. *Cell* 2012;149:656–670.
26. Del Poggetto E, Ho IL, Balestrieri C, et al. Epithelial memory of inflammation limits tissue damage while promoting pancreatic tumorigenesis. *Science* 2021;373(6561):eabj0486.
27. Cobo I, Iglesias M, Flandez M, et al. Epithelial *Nr5a2* heterozygosity cooperates with mutant *Kras* in the development of pancreatic cystic lesions. *J Pathol* 2021;253:174–185.
28. Moreno CS. *SOX4*: The unappreciated oncogene. *Semin Cancer Biol* 2020;67:57–64.
29. Burdziak C, Alonso-Curbelo D, Walle T, et al. Epigenetic plasticity cooperates with cell-cell interactions to direct pancreatic tumorigenesis. *Science* 2023;380(6645):ead5327.
30. DelGiorno KE, Naeem RF, Fang L, et al. Tuft cell formation reflects epithelial plasticity in pancreatic injury: implications for modeling human pancreatitis. *Front Physiol* 2020;11:88.
31. Westphalen CB, Takemoto Y, Tanaka T, et al. *Dclk1* defines quiescent pancreatic progenitors that promote injury-induced regeneration and tumorigenesis. *Cell Stem Cell* 2016;18:441–455.
32. Bailey JM, Alsina J, Rasheed ZA, et al. *DCLK1* marks a morphologically distinct subpopulation of cells with stem cell properties in preinvasive pancreatic cancer. *Gastroenterology* 2014;146:245–256.
33. Carpenter ES, Elhossiny AM, Kadiyala P, et al. Analysis of donor pancreata defines the transcriptomic signature and microenvironment of early neoplastic lesions. *Cancer Discov* 2023;13:1324–1345.
34. DelGiorno KE, Chung CY, Vavinskaya V, et al. Tuft cells inhibit pancreatic tumorigenesis in mice by producing prostaglandin *D*₂. *Gastroenterology* 2020;159:1866–1881.
35. Hoffman MT, Kemp SB, Salas-Escabillas DJ, et al. The gustatory sensory G-protein *GNAT3* suppresses pancreatic cancer progression in mice. *Cell Mol Gastroenterol Hepatol* 2021;11:349–369.
36. Salas-Escabillas DJ, Hoffman MT, Moore JS, et al. Metaplastic tuft cells transdifferentiate to neural-like progenitor cells in the progression of pancreatic cancer. *bioRxiv Preprint* posted online April 23, 2024. <https://doi.org/10.1101/2024.02.12.579982>.
37. von Moltke J, Ji M, Liang HE, et al. Tuft-cell-derived *IL-25* regulates an intestinal *ILC2*-epithelial response circuit. *Nature* 2016;529(7585):221–225.

38. Blasco MT, Navas C, Martin-Serrano G, et al. Complete regression of advanced pancreatic ductal adenocarcinomas upon combined inhibition of EGFR and C-RAF. *Cancer Cell* 2019;35:573–587.
39. Espinet E, Gu Z, Imbusch CD, et al. Aggressive PDACs show hypomethylation of repetitive elements and the execution of an intrinsic IFN program linked to a ductal cell of origin. *Cancer Discov* 2021;11:638–659.
40. Lo EKW, Mears BM, Maurer HC, et al. Comprehensive DNA methylation analysis indicates that pancreatic intraepithelial neoplasia lesions are acinar-derived and epigenetically primed for carcinogenesis. *Cancer Res* 2023;83:1905–1916.
41. Velez-Delgado A, Donahue KL, Brown KL, et al. Extrinsic KRAS signaling shapes the pancreatic microenvironment through fibroblast reprogramming. *Cell Mol Gastroenterol Hepatol* 2022;13:1673–1699.
- Anita Kurilla, PhD (Investigation: Supporting)
H. Carlo Maurer, MD (Data curation: Supporting; Formal analysis: Supporting; Investigation: Supporting; Methodology: Supporting)
Sebastian Arcila-Barrera, PhD (Data curation: Supporting)
Xinyi Lin (Investigation: Supporting)
Zhaolong Pan, PhD (Investigation: Supporting)
Joana Leitão Castro, MSc (Investigation: Supporting; Methodology: Supporting)
Alejandro Enrique Mayorca-Guiliani, MD, PhD (Investigation: Supporting; Methodology: Supporting)
Charlotte Vestrup Rift, MD, PhD (Resources: Supporting)
Jane Hasselby, MD, PhD (Resources: Supporting)
Luc Bouwens, PhD (Resources: Supporting)
Véronique Lefebvre, PhD (Resources: Supporting)
Charles J. David, PhD (Investigation: Supporting)
Oren Parnas, PhD (Investigation: Supporting)
Kathleen E. DelGiorno, PhD (Data curation: Supporting; Resources: Supporting; Visualization: Supporting)
Janine Terra Erler, PhD (Methodology: Supporting; Resources: Supporting)
Ilse Rooman, PhD (Methodology: Supporting; Resources: Supporting)
Luis Arnes, PhD (Conceptualization: Lead; Funding acquisition: Lead; Project administration: Lead; Supervision: Equal; Visualization: Lead; Writing – original draft: Lead; Writing – review & editing: Lead)

Conflicts of interest

The authors disclose no conflicts.

Funding

This work was supported by the Danish Cancer Society (R302-A17481, R352-A20566). Jonathan Baldan is supported by a Foundation Against Cancer Fundamental mandate (2023-038). Joana Leitão Castro is funded by the European Union's Horizon 2020 research and innovation program under the Marie Skłodowska-Curie grant agreement No. 101034291 (DISCOVER). Anita Kurilla is funded by the European Union's Horizon 2020 research and innovation program under the Marie Skłodowska-Curie grant agreement No. 945322 (LEAD). Kathleen E. DelGiorno is supported by the Vanderbilt-Ingram Cancer Center (National Institutes of Health [NIH]/National Cancer Institute [NCI] P30 CA068485), the Vanderbilt Digestive Disease Research Center (NIH/National Institute for Digestive and Kidney Diseases P30 DK058404), the Vanderbilt-Ingram Cancer Center Specialized Program of Research Excellence (SPORE) in Gastrointestinal Cancer (NIH/NCI 5P50 CA236733), the American Gastroenterological Association Research Scholar Award (AGA2021-13), the Department of Defense (W81XWH221121), and NIH/National Institute of General Medical Sciences R35 GM142709. Véronique Lefebvre is supported by NIH/National Institute of Arthritis and Musculoskeletal and Skin Diseases grants R01 AR068308, AR072649, and AR080062. Ilse Rooman is supported by the Research Foundation Flanders (FWO) (FWO research project G001619N; Odysseus fellowship G0F8916N). Luis Arnes is supported by core funding of the Biotech Research and Innovation Center, the Danish Cancer Society (R352-A20566, R302-A17481, R322-A17.350), the Novo Nordisk Foundation (NNF21OC0070884), and the Innovation Fund (Eurostars 2807). The Novo Nordisk Foundation Center for Stem Cell Biology was supported by Novo Nordisk Foundation grants NNF17CC0027852.

Data Availability

The transcriptomic and sequencing data discussed in this publication have been deposited in the Gene Expression Omnibus archive (GSE154628, GSE235809).

Received June 26, 2023. Accepted April 29, 2024.

Correspondence

Address correspondence to: Luis Arnes, PhD, University of Copenhagen, Biotech Research and Innovation Centre, Ole Maaloes Vej 5, 2300 Copenhagen, Denmark. e-mail: luis.arnes@bric.ku.dk; or Jonathan Baldan, PhD, Translational Oncology Research Center, Vrije Universiteit Brussel (VUB), Brussels, Laarbeeklaan 103, 1090, Brussels, Belgium. e-mail: Jonathan.baldan@vub.be.

Acknowledgments

The authors extend their sincere gratitude to Christopher Wright for providing the Ptf1aCreER mice. We also thank the core facilities at the Biotech Research and Innovation Centre, University of Copenhagen, especially Juliana Assis and Leonor Rib in Bioinformatics, Mia Kristine in Histocore, Irina Korshunova in 10× Genomics Single Cell, and Rajesh Somasundaram in Flow Cytometry. Their invaluable support and expertise have significantly contributed to the success of this research. The authors are grateful for the service provided by Visual and Spatial Tissue Analysis (<https://vsta.research.vub.be>). The graphical abstract was created with BioRender.com. Jonathan Baldan's current affiliation is with the Translational Oncology Research Center, Vrije Universiteit Brussel, Brussels, Belgium.

CRedit Authorship Contributions

Jonathan Baldan, PhD (Conceptualization: Equal; Data curation: Lead; Formal analysis: Lead; Investigation: Lead; Methodology: Lead; Supervision: Equal; Visualization: Supporting; Writing – original draft: Equal; Writing – review & editing: Supporting)

Juan Camacho-Roda, MSc (Data curation: Supporting; Investigation: Supporting; Methodology: Supporting)

Marta Ballester, MSc (Data curation: Supporting; Formal analysis: Supporting; Investigation: Supporting; Methodology: Supporting)

Kristina Hoj, MSc (Investigation: Supporting)

Supplementary Methods

Mouse Models

LSL-KrasG12D (MGI:2429948), Ptf1aCreER (MGI:3771322), R26RYFP (MGI:2449038), and Sox4flox (MGI:3773012) mouse strains were used for breeding. Mice were maintained on a genetically mixed background. Animals were housed in accordance with best animal husbandry guideline recommendations of the European Union Directive (2010/63/EU). The Danish Animal Experiments Inspectorate reviewed and approved all animal experiments.

In Vivo Mouse Experiments

Tamoxifen (T5648, Sigma-Aldrich) was administered through intraperitoneal injections every other day for 5 days (eg, Monday, Wednesday, Friday) at a dose of 3 mg per injection. Tamoxifen was dissolved in corn oil (C8267, Sigma-Aldrich) at a stock concentration of 30 mg/mL (100 μ L/injection). A standard wash-out of 2 weeks was performed. To induce tissue injury in the pancreas, the cholecystokinin analogue caerulein (C9026, Sigma-Aldrich) was administered through intraperitoneal injections every hour for 7 hours (8 injections/day) on 2 consecutive days at a concentration of 125 μ g/kg body weight, as described elsewhere.⁴⁰ Control mice were injected with equivalent volume of phosphate-buffered saline (PBS) following the same protocol.

RNA Extraction and Complementary DNA

Synthesis of Pancreatic Tissue

RNA was extracted using the RNeasy Mini Kit (Qiagen, no. 74106) according to the manufacturer's instructions for high-content RNase tissues. The extracted RNA's concentration and sample quality were measured using a spectrophotometer (DeNovix, DS-11). Retrieved RNA was treated with DNase to remove genomic DNA (Invitrogen, no. 18068015). Samples were stored at -80°C . Complementary DNA (cDNA) was synthesized using the GoScript Reverse Transcription System kit (Promega, no. A5001).

Flow Cytometry

The isolated cells were incubated with L/D fixable violet or red dyes (Thermo Fisher Scientific; violet: L34955, red: L34971) and then stained with the surface antibody cocktail for 30 minutes at room temperature protected from light (Supplementary Table 7). Solenocytes from the spleen were used as the fluorescence minus one. Cells were centrifuged for 5 minutes at 300g and fixed using Fix-Perm Solution (Thermo Fisher Scientific, 00-5523-00) for 30 minutes at room temperature. Finally, cells were washed with wash buffer (from the Fix-Perm kit), centrifuged for 5 minutes at 600g, and resuspended with staining buffer (fetal bovine serum [FBS] 2% in PBS). Centrifuges were performed for 5 minutes at 600g.

Flow cytometry was performed on an LSRFortessa X20 (BD Biosciences). For spleen, 500,000 events were recorded, and between 1 and 2 million were recorded for pancreas.

Cytometry data were analyzed with FlowJo 20 (Treestar Inc) using conventional manual gating.

Compensation was calculated using Ultracomp eBeads Compensation Beads (Thermo Fisher Scientific, 01-2222-41) and Arc Amine Reactive Compensation Bead Kit (Thermo Fisher Scientific, A10628).

Quantitative Reverse Transcription Polymerase Chain Reaction

Expression levels were calculated using the comparative delta-delta cycle threshold method of relative quantitation, with *Rpl5* (ribosomal protein L5) and *Rps29* (ribosomal protein S2) as housekeeping genes for mouse samples and *PPIA* (peptidylprolyl isomerase A) for human samples (Supplementary Table 7).

Immunohistochemistry and Immunofluorescence

Pancreata were fixed in 4% paraformaldehyde (VWR Chemicals, 9713-1000) for 24 hours at room temperature and kept in 70% ethanol at room temperature (VWR Chemicals, 20824.365) until paraffin embedding or 30% sucrose for cryoprotection in optimal cutting temperature compound. Tissues were cut into 4- to 10- μ m sections and placed on Superfrost Plus slide (Thermo Fisher Scientific, 10149870). Antigen retrieval was performed with Tris-EDTA buffer at pH 9.0. Sections were washed in PBS-Tween 0.5% and blocked with 1% donkey serum before incubation with primary antibodies overnight at 4°C . Secondary antibodies plus DAPI were incubated for 1 hour at room temperature. Sections were mounted with Vectashield Mounting medium (Vector Laboratories, H-1000). The list of antibodies can be found in Supplementary Table 7.

Acinar-to-Ductal Metaplasia Quantification

For the quantification of ADM, we used whole pancreas scans stained with H&E and applied color deconvolution tools using QuPath v.0.4.1 (Queen's University, Belfast, Northern Ireland). After manually excluding arteries, connective tissue, fat, lymph nodes, and staining artifacts, we annotated the acinar tissue using the Threshold tool, which calculates the average of all channels. Subsequently, we used a pixel classifier trained with random trees to further eliminate edema and infiltration. The results are expressed as the percentage of ADM.

RNA In Situ Hybridization

RNAscope Multiplex Fluorescent Reagent Kit version 2 (ACD Bio) was used, following the manufacturer's instructions. Paraffin sections were rehydrated and incubated with hydrogen peroxide, and target retrieval was performed for 15 minutes. Protease III was applied for 15 minutes, and each section was incubated with the RNAscope Probe-Mm-Sox4 (ACD Bio, 471381) or RNAscope Probe-Hs-SOX4 (ACD Bio, 469911) for 2 hours. Standard hybridization (concentration of 1:1500) and subsequent immunofluorescence (IF) staining were performed as previously described. Slides were mounted with Prolong Gold Antifade Reagent

(Cell Signaling, 9071S) and imaged with the Olympus ScanR screening or Zeiss AxioScan.

Decellularization Procedure

Mice were killed by suffocation with CO₂, shaved, and disinfected with 70% ethanol. Each mouse was pinned supine to a polystyrene tray and examined under a surgical microscope (Leica S6D, Leica). The aorta was catheterized using a 26-gauge catheter, and a stitch was placed 1 cm above the tip of the catheter to secure it and prevent backflow. The arterial celiac trunk was ligated by placing a 9-0 suture immediately below its emergence. Decellularization of the pancreas was performed through the perfusion of 150 μ L/min of 0.5% deoxycholic acid (Sigma) for 24 hours, carried out with a peristaltic pump (Ole Dich). Sterile Milli-Q water was then perfused for 18 hours to remove the detergent before switching to PBS for another 6 hours. The decellularized pancreas were carefully extracted and stored in PBS until staining. Sections of the decellularized pancreas were placed inside a cryotube containing a blocking solution of 6% donkey serum and 3% (weight/volume) bovine serum albumin in PBS. Samples were incubated on a rocking table (~15 revolutions/min at room temperature for all experiments) overnight. Primary antibody solutions (1:100 primary antibody, in 3% donkey serum in PBS) were added, and the samples were incubated for 24 hours. Samples were washed in a washing solution (0.05% Tween20 in PBS) for 1 hour 5 times. A secondary antibody solution (1:1000 secondary antibody in 3% donkey serum in PBS) was added, and pancreata were incubated overnight. Three washing cycles of 1 hour were performed with the washing solution. Negative control samples were generated through the same procedure but without the primary antibody. Images were obtained on the inverted confocal microscope (Leica SP5-X, Leica, Germany).

RNA Sequencing and Data Analysis

Samples with an RNA integrity number of >7 were sent for RNA sequencing analysis to Novogene. After a library quality control, sequencing was performed using the Illumina NovaSeq 6000 platform, pair-end 150 base pair sequencing, with a depth of 20 million read pairs per sample. Bioinformatic analysis was provided by Novogene unless otherwise indicated.

Fast Green and Sirius Red

Paraffin embedded tissues were deparaffinized and stained with Fast Green and Sirius Red solution for 1 hour (1 mg/ml Fast Green, Sigma-Aldrich F7258-25G; 1 mg/ml Direct Red 80, Sigma-Aldrich 365548-25G; 1.3% in water Picric acid, Merck P6744-1GA). Sections were then dehydrated with ethanol and xylene and mounted with entellan (EMD Millipore, 1.0790.0500).

Human Explants and Microarray

Anonymized donor pancreata were obtained from the Beta Cell Bank of the JDRF Centre for Beta Cell Therapy in

Diabetes. Full written consent for use of donor material for research was obtained. Isolation of the exocrine cell fraction was performed as previously described.⁴⁰ cDNA was prepared using the GeneChip WT PLUS Reagent kit and hybridized onto the GeneChip Human Gene 2.0 ST Array (Affymetrix). Quality control and data normalization were conducted using the transcriptome analysis console (Thermo Fisher Scientific). Differences were determined as significant when the false discovery rate *P* value was less than or equal to .05 and the fold change was >2 and <-2.

Single-Cell Suspension

Pancreas tissue was finely chopped with scissors in digestion buffer (1 mg/mL Collagenase (Sigma-Aldrich, C9407-1G), 1 mg/mL DNase I (Sigma-Aldrich, 11284932001), 0.1 mg/mL soybean trypsin inhibitor (Thermo Fisher Scientific, 17-075-029) dissolved in Hank's balanced salt solution (HBSS). Digestion was performed in gentleMACS C Tubes using the mTDK1 program on a gentleMACS Dissociator (Miltenyi Biotec). The reaction was stopped with STOP buffer (1 mg/mL DNase I [Sigma-Aldrich, 11284932001], 0.1 mg/mL soybean trypsin inhibitor, and 5% FBS dissolved in HBSS). Digested tissue was centrifuged for 5 minutes at 2000 revolutions/min and resuspended in 3 mL RBC lysis buffer (Thermo Fisher Scientific, 00-4333-57). After 2 minutes incubation cells were washed with STOP buffer twice and filtered through a 40- μ m cell strainer. Cells were then resuspended in fluorescence-activated cell sorter buffer (1 mg/mL DNase I [Sigma-Aldrich, 11284932001] and 1% FBS dissolved in HBSS) before staining.

Single-Cell RNA Sequencing

Single-cell dissociation was prepared as described in the "Single-Cell Suspension" section with some changes. An additional digestion step with Trypsin-EDTA (Thermo Fisher Scientific, 25-200-056) diluted 1:5 in cell suspension was performed before the RBC lysis. After collection, the cells were centrifuged at a speed not exceeding 400 relative centrifugal force. The supernatant was discarded. The cell pellet was resuspended in 1 mL 1 \times PBS containing 0.04% bovine serum albumin, and the washing procedure was repeated twice. After washing, an appropriate volume of PBS was added to the cell precipitation to obtain single-cell dispersion suspension with a concentration close to the goal number. A wide-bore pipette tip was used for pipetting cell resuspension for lower cell damage, and 40- μ m cell strainers were used for removing cell debris and cell clumps. Automatic cytometry was used to determine the cell concentration. The sample volume was calculated based on the optimal cell sampling concentration supplied by the 10 \times Genomics official website and the target capture number. If the calculated concentration was too high, the liquid volume was adjusted to the appropriate concentration, and the counting was repeated. Once the desired cell suspension was obtained, it was immediately placed on ice for subsequent gel beads-in-emulsion preparation and reverse transcription.

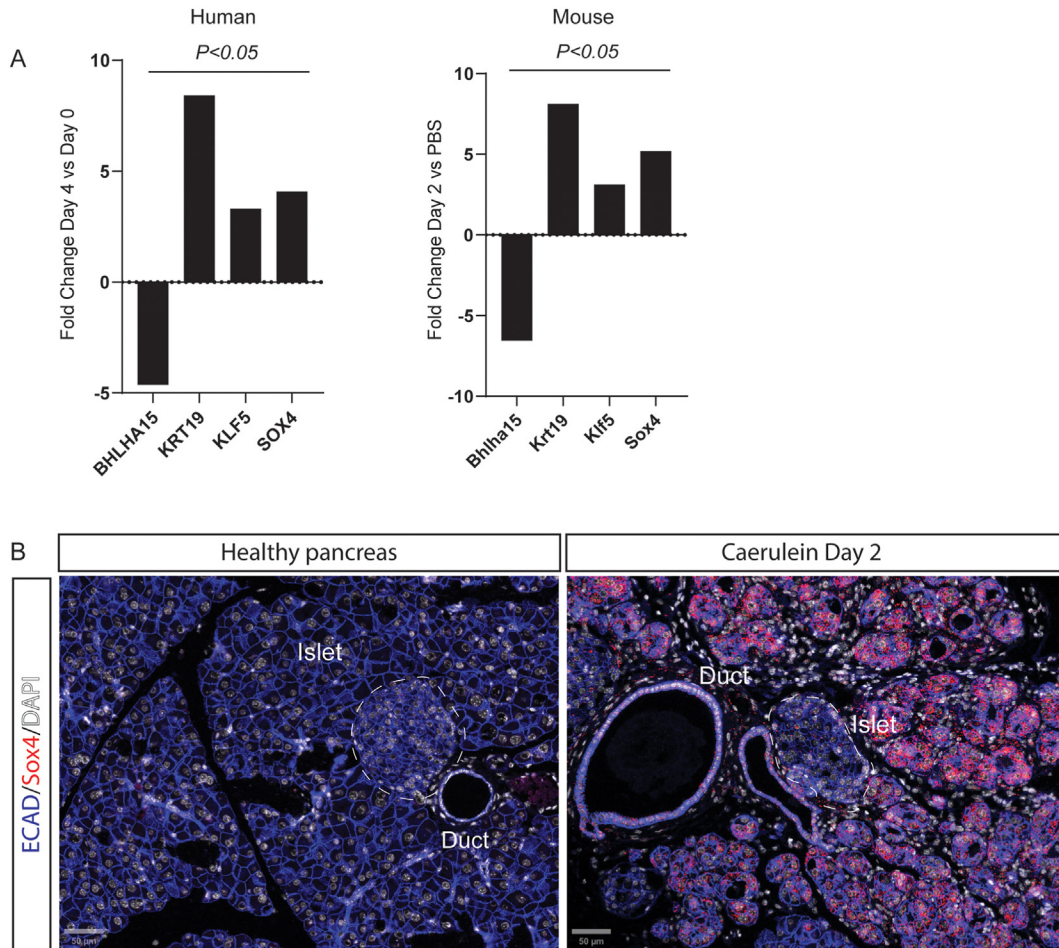
10× Genomics Library Preparation and Sequencing

Chromium Single Cell 3' Reagent Kits version 3.1 Dual Index (10× Genomics, PN-1000268) were used for library preparation according to a standard protocol. In brief, cells were counted under a microscope, mixed with reverse transcription mix, and partitioned together with v3 Gel Beads on Chromium Chip B (10× Genomics, PN-1000127) into gel beads in emulsion using Chromium Controller (10× Genomics, PN-120223). After reverse transcription, samples were frozen at -20°C . Within a week, samples from several 10× runs were processed together for cDNA cleanup and preamplification (12 polymerase chain reaction [PCR] cycles). After SPRIselect (Beckman Coulter) cleanup, cDNA was quantified and frozen at -20°C . In general, the same quantity of cDNA was used during fragmentation, end repair, and A-tailing for most samples. After this, fragments were cleaned up using SPRIselect reagent and processed through the steps of adapter ligation, SPRIselect cleanup, and sample index PCR (using Chromium i5 and i7 Sample Indices [10× Genomics, PN-1000215] for 11 PCR cycles). After this, libraries were cleaned up with SPRIselect reagent and quantified using the Qubit HS dsDNA Assay Kit (Thermo Fisher Scientific, Q32854) and Qubit Fluorometer and also using the High Sensitivity D5000 Reagents (Agilent, 5067-5593) and

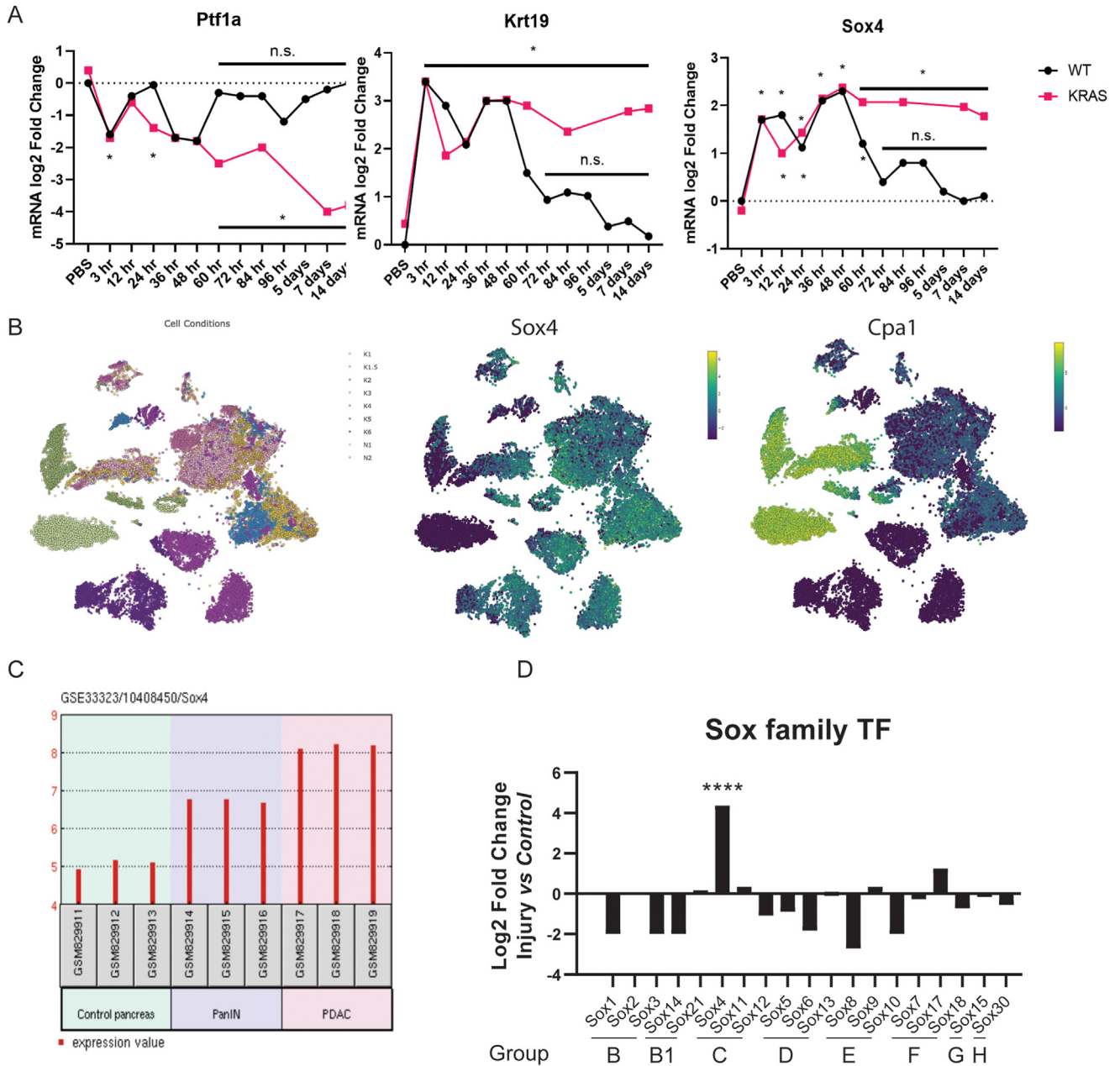
Agilent 4150 TapeStation. Libraries were pooled according to the expected amount of cells per sample; each pool was quantified and sequenced using 100 cycles of NovaSeq 6000 S2 (Illumina, 20028316) runs on Illumina NovaSeq 6000 System (Illumina 20012850) controlled by NovaSeq control software. Libraries were sequenced using 28 cycles for read 1, 10 cycles for the i7 index, 10 cycles for the i5 index, and 90 cycles for read 2.

Supplementary References

- e1. [Kong B, Bruns P, Behler NA, et al. Dynamic landscape of pancreatic carcinogenesis reveals early molecular networks of malignancy. *Gut* 2018;67:146–156.](#)
- e2. [Burdziak C, Alonso-Curbelo D, Walle T, et al. Epigenetic plasticity cooperates with cell-cell interactions to direct pancreatic tumorigenesis. *Science* 2023;380\(6645\): eadd5327.](#)
- e3. [Alonso-Curbelo D, Ho YJ, Burdziak C, et al. A gene-environment-induced epigenetic program initiates tumorigenesis. *Nature* 2021;590\(7847\):642–648.](#)
- e4. [Ma Z, Lytle NK, Chen B, et al. Single-cell transcriptomics reveals a conserved metaplasia program in pancreatic injury. *Gastroenterology* 2022;162:604–620.](#)

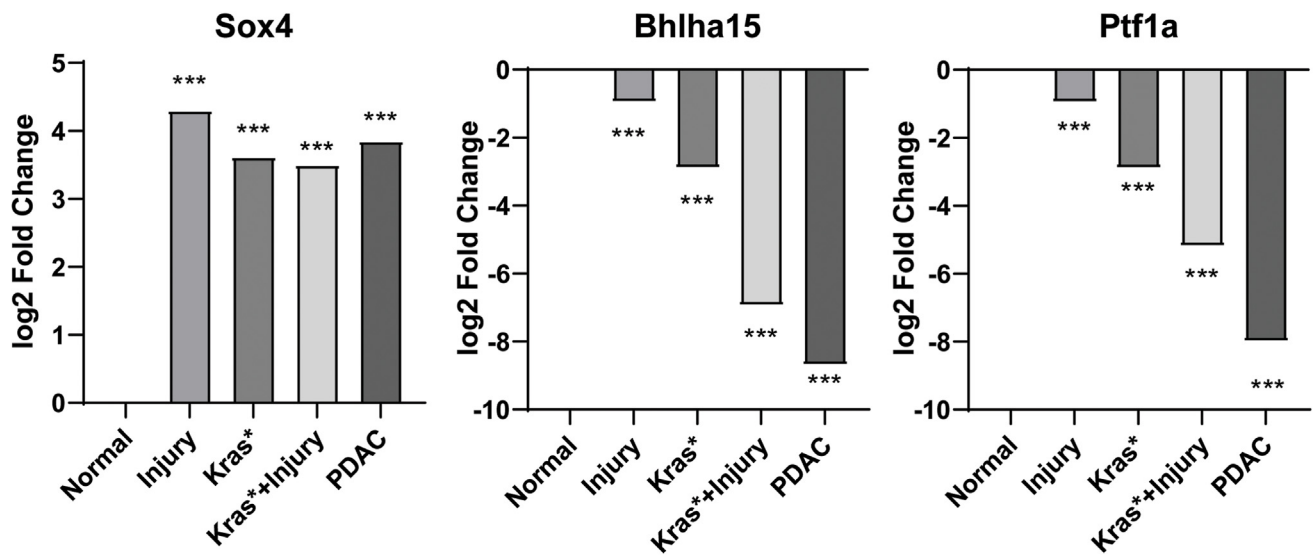


Supplementary Figure 1. *Sox4* expression is associated with pancreatic injury. (A) Gene expression analysis in freshly isolated mouse exocrine pancreas the day of isolation and after 4 days in culture. (B) ISH and immunofluorescence analysis in the pancreas 2 days after caerulein-induced pancreatitis. The expression of *Sox4* is restricted to the ADM and ductal cells. Representative images of at least 3 mice. Scale bar, 50 μ m. DAPI, 4',6-diamidino-2-phenylindole.



Supplementary Figure 2. *Sox4* expression pattern analysis in experimental mouse models of pancreas regeneration and cancer initiation. (A) Microarray gene expression analysis^{e1} of *Sox4* and markers of ADM (*Krt19*) and acinar differentiation (*Ptf1a*) with temporal resolution in *P48cre/+; LSL-KrasG12D/+* and WT mice. (B) UMAP plots of scRNAseq profiles of mouse epithelial cells at different stages of PDAC progression from normal acinar cells. (Left) Colored by sample. (Middle and right) colored by the expression of *Sox4* and *Cpa1*.^{e2} (C) *Sox4* expression in the pancreas, PanINs, and PDAC assessed in RNA sequencing from mouse pancreas. (D) Gene expression analysis^{e3} of the Sox family of transcription factors in lineage-traced acinar cells 4 days after caerulein-induced pancreatitis. UMAP, uniform manifold approximation and projection. TF, transcription factor.

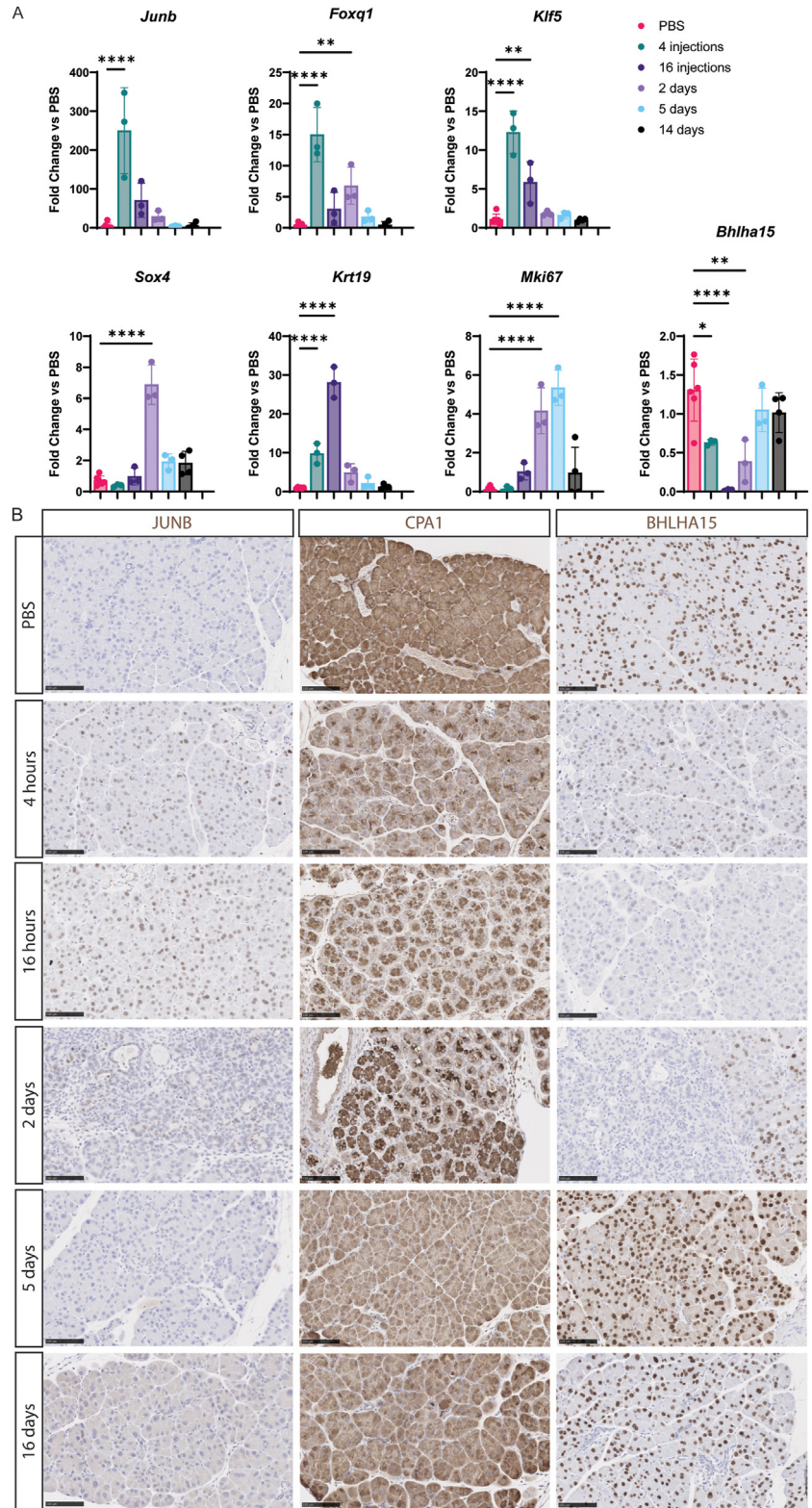
A



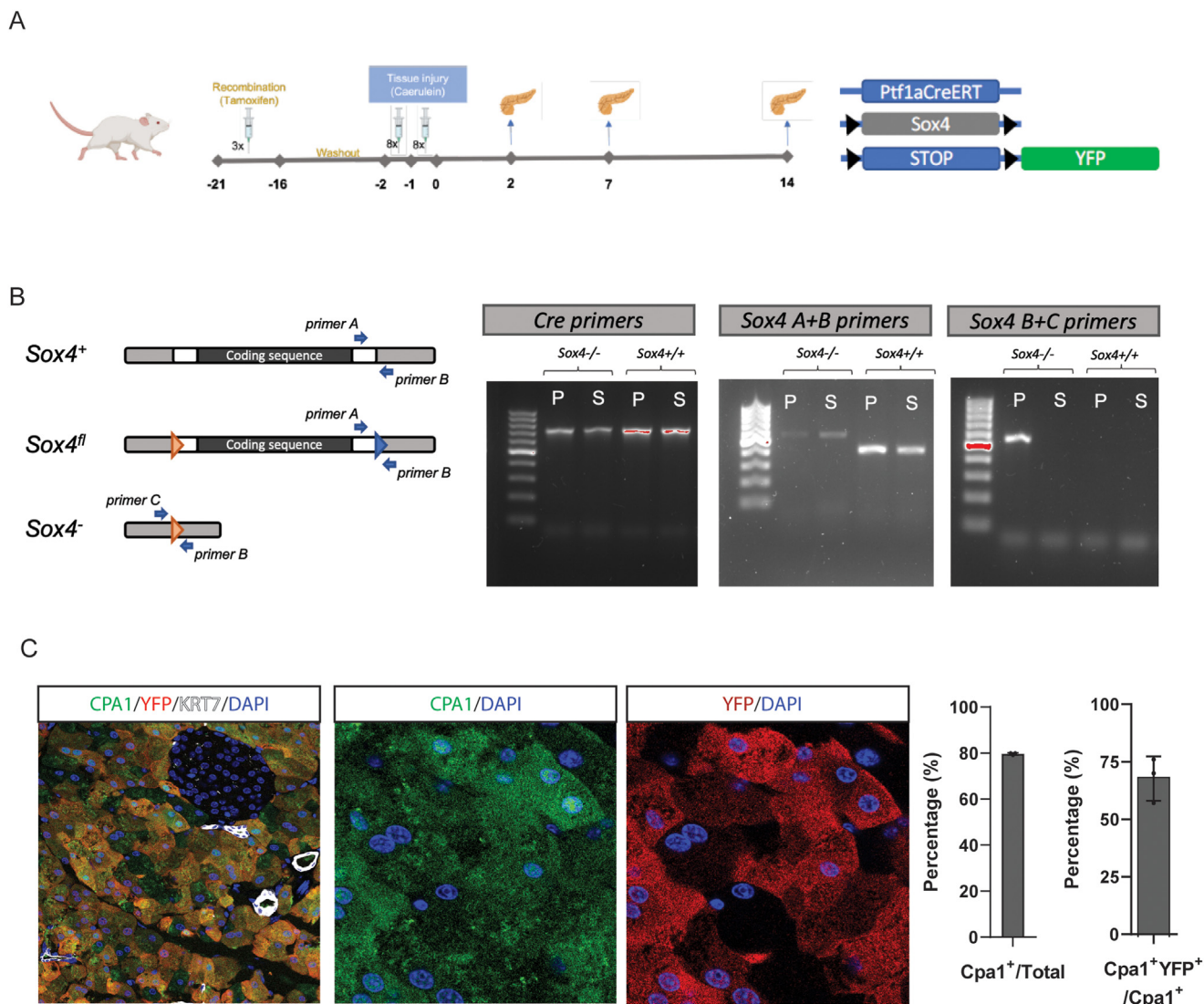
B



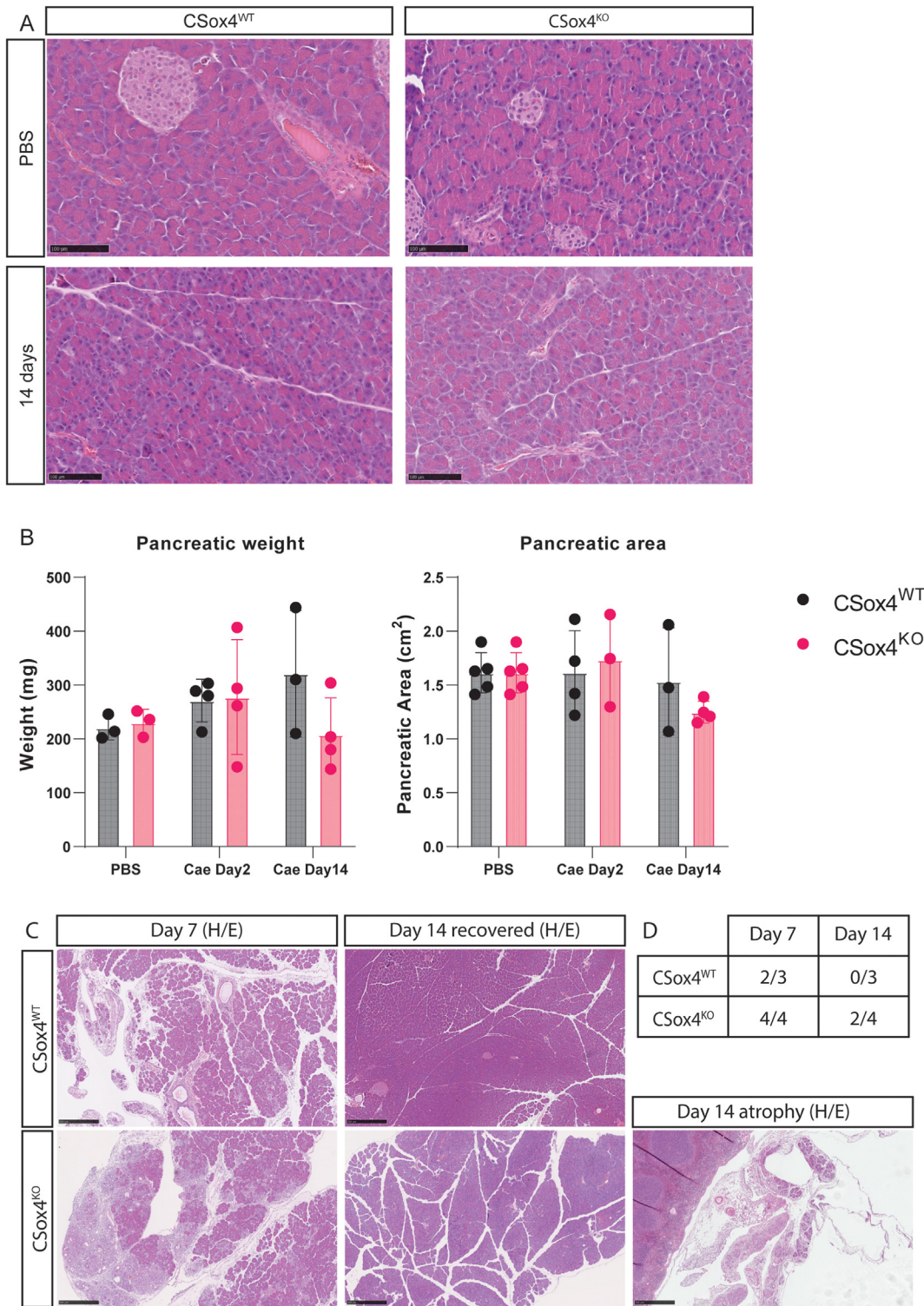
Supplementary Figure 3. Sox4 expression increases in tissue injury and disease progression. (A) Gene expression analysis of the Sox4 locus in sorted lineage-traced acinar cells during disease progression in mouse PDAC by RNA sequencing. (B) Expression pattern of SOX4 and metaplastic markers in scRNAseq from human chronic pancreatitis.



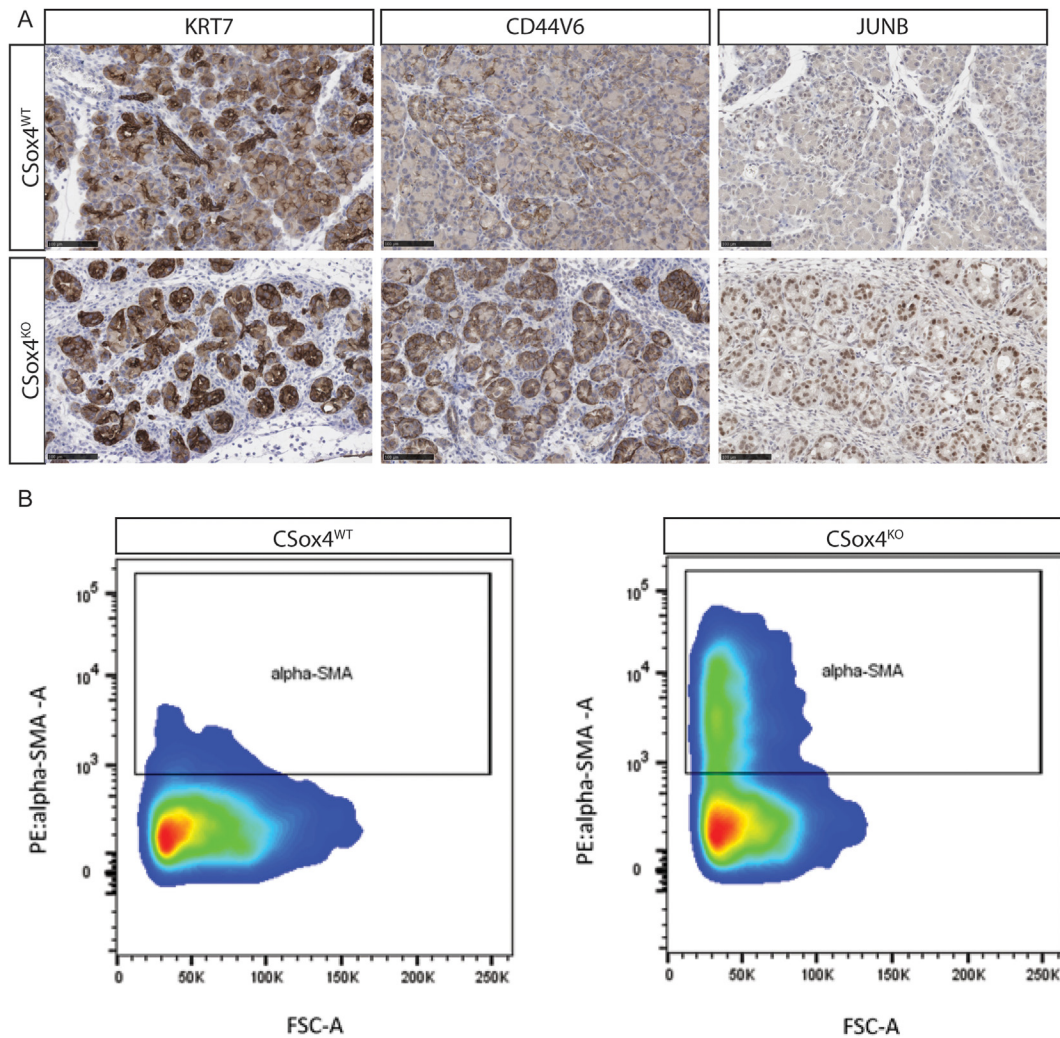
Supplementary Figure 4. *Sox4* expression peaks after ADM and concomitant with proliferation in caerulein-induced pancreatitis. (A) We investigated the expression pattern of *Sox4* in relation to markers of ADM, proliferation, and acinar identity with temporal resolution in pancreas regeneration using quantitative PCR. *Sox4* expression is up-regulated after *Junb*, *Foxq1*, and *Klf5* and coincides with the recovery of acinar markers and proliferation. * $P < .05$, ** $P < .01$, *** $P < .001$ vs PBS. Error bars represent standard deviation (SD). Ordinary 1-way analysis of variance with multiple comparison test vs PBS samples ($n \leq 3$). (B) Expression pattern of metaplastic and acinar differentiation markers in the progression and resolution of experimental pancreatitis. Immunohistochemical analysis of *Junb*, carboxypeptidase A1, and *Bhlha15* in the pancreas of C57bl6 mice after caerulein injection and PBS control. Images are representative of at least 3 mice. Scale bar, 100 μm .



Supplementary Figure 5. Acinar-specific allele recombination. (A) Schematic representation of the experimental procedure. We injected 3 mg of tamoxifen intraperitoneally on 3 alternate days in CSox4^{WT} and CSox4^{KO} mice. After 2 weeks of washout, mice were subjected to a 2-day protocol of 8 hourly intraperitoneal injections of caerulein to induce pancreatic injury and inflammation. Tissues were extracted at the indicated timepoints for histologic and molecular analysis. Image created with Biorender (<https://biorender.com/>). (B) Schematic representation of the modified Sox4 allele indicating the relative position of the primers used for genotyping and analysis of pancreas-specific recombination. We confirmed the specificity of Sox4 deletion in the pancreas by PCR amplification of DNA from pancreas and spleen. (C) We performed immunofluorescence analysis to determine the fraction of YFP⁺ cells in the pancreas after 2 weeks of tamoxifen washout. We observed labeling efficiency of 67.2% ± 10.6% (n = 3), which was specific to the acinar cells. Representative images of at least 3 mice are shown. Error bars represent standard deviation. Original magnification, 40× (left) and 80× (middle and right). DAPI, 4',6-diamidino-2-phenylindole.

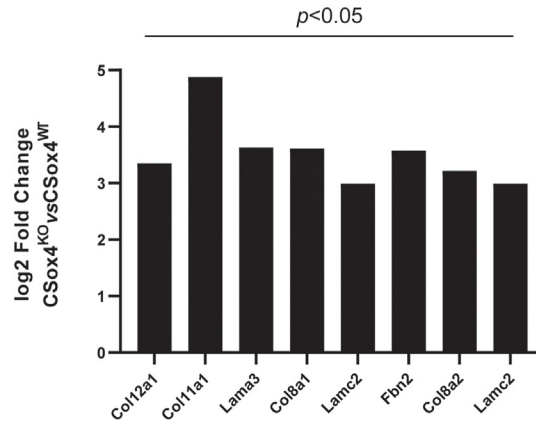


Supplementary Figure 6. *Sox4* is dispensable for tissue homeostasis. (A) We performed histologic analysis of the pancreas resected after 14 days of caerulein injection and PBS control. Scale bar, 100 μ m. (B) The pancreas recovered its size and weight after experimental pancreatitis in CSox4^{WT} and CSox4^{KO} mice. (C) Representative histologic images of pancreatic tissue post-caerulein-induced pancreatitis in both CSox4^{WT} and CSox4^{KO} mice. The image for CSox4^{KO} at day 14 exemplifies the observed tissue damage in 2 out of the 4 mice, illustrating the variability in response to *Sox4* deletion. Scale bar, 500 μ m. (D) Pathologist's evaluation of histologic evidence of pancreatitis in both CSox4^{WT} and CSox4^{KO} mice. It is important to highlight that the impact of *Sox4* deletion on tissue regeneration is not observed across all specimens. This partial recovery in some mice suggests the presence of more complex, perhaps compensatory, mechanisms governing tissue homeostasis and recovery. CAE, caerulein; H/E, hematoxylin and eosin.

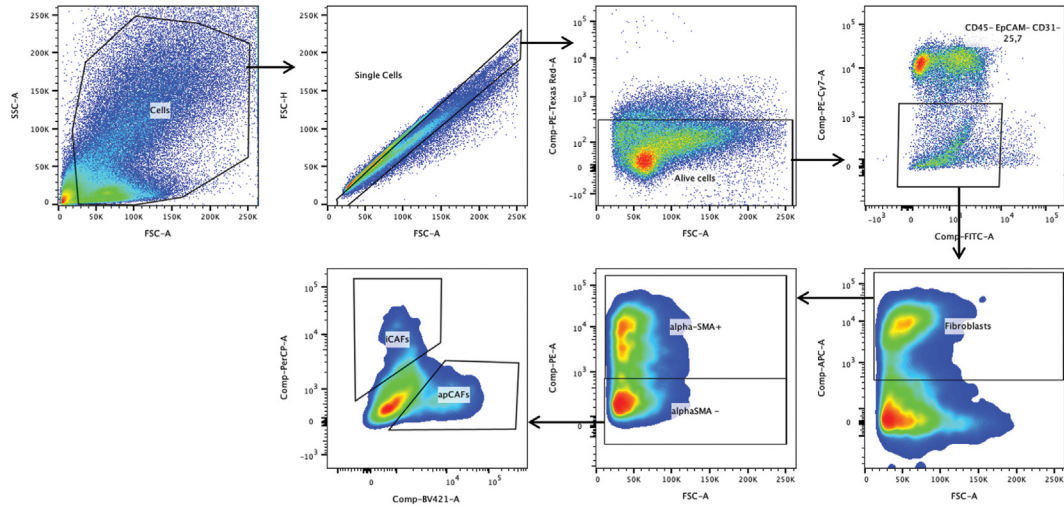


Supplementary Figure 7. *Sox4* restricts the tissue damage response in the pancreas. (A) We performed DAB staining with markers of acinar metaplasia 2 days after the injection of the first dose of caerulein. Scale bar, 100 μ m. (B) Representative flow cytometry image of α SMA⁺ fibroblasts 2 days postinjury in CSox4^{WT} and CSox4^{KO} mice. Sox4 deletion in acinar cells increased the number of activated myCAFs in the tissue. Experiment was performed in 6 animals per group. (C) Gene expression analysis showed up-regulation of extracellular matrix proteins in CSox4^{KO} compared to CSox4^{WT} mice. (D, E) We investigated the different subtypes of CAFs 2 days after caerulein-induced injury using flow cytometry. Representative flow cytometry gating strategy for quantification of myCAFs (CD326⁻CD31⁻CD45⁻PDPN⁺ α SMA⁺), iCAFs (CD326⁻CD31⁻CD45⁺PDPN⁺ α SMA⁻Ly6C⁺MHCII⁻), and apCAFs (CD326⁻CD31⁻CD45⁻PDPN⁺ α SMA⁻Ly6C⁻MHCII⁺) (D). FMO controls were used to assess background and set the gatings for flow cytometry analysis (E). APC, allophycocyanin; apCAF, antigen-presenting cancer-associated fibroblast; CAF, cancer-associated fibroblast; DAB, 3,3'-diaminobenzidine tetra hydrochloride; FMO, fluorescence minus one; PDPN, podoplanin; PE, phycoerythrin; PerCP, peridinin-chlorophyll-protein.

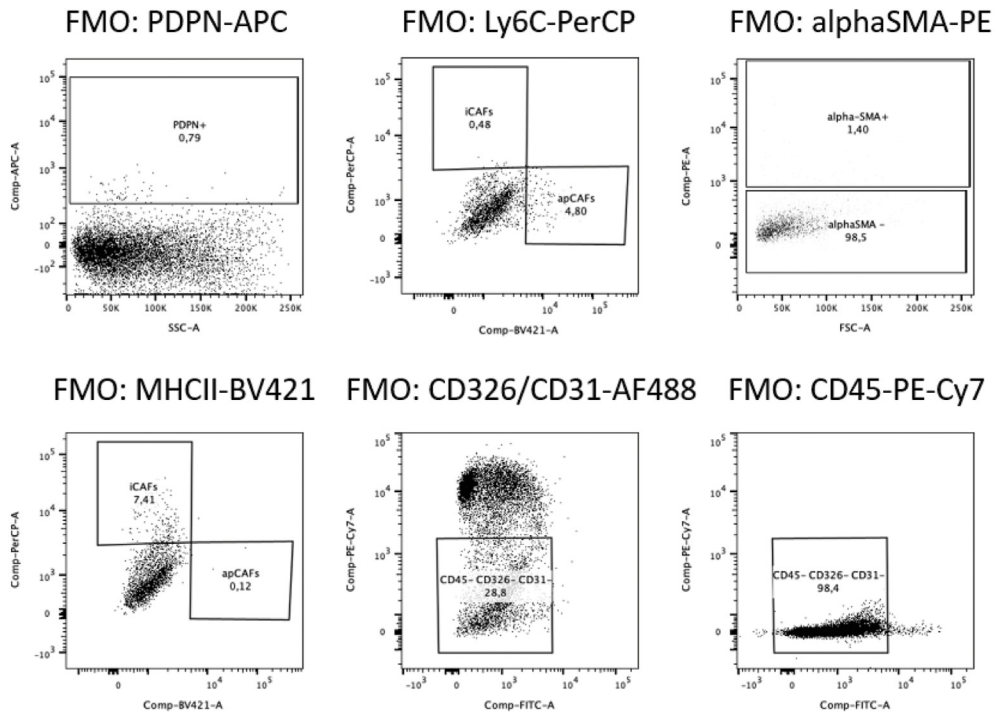
C



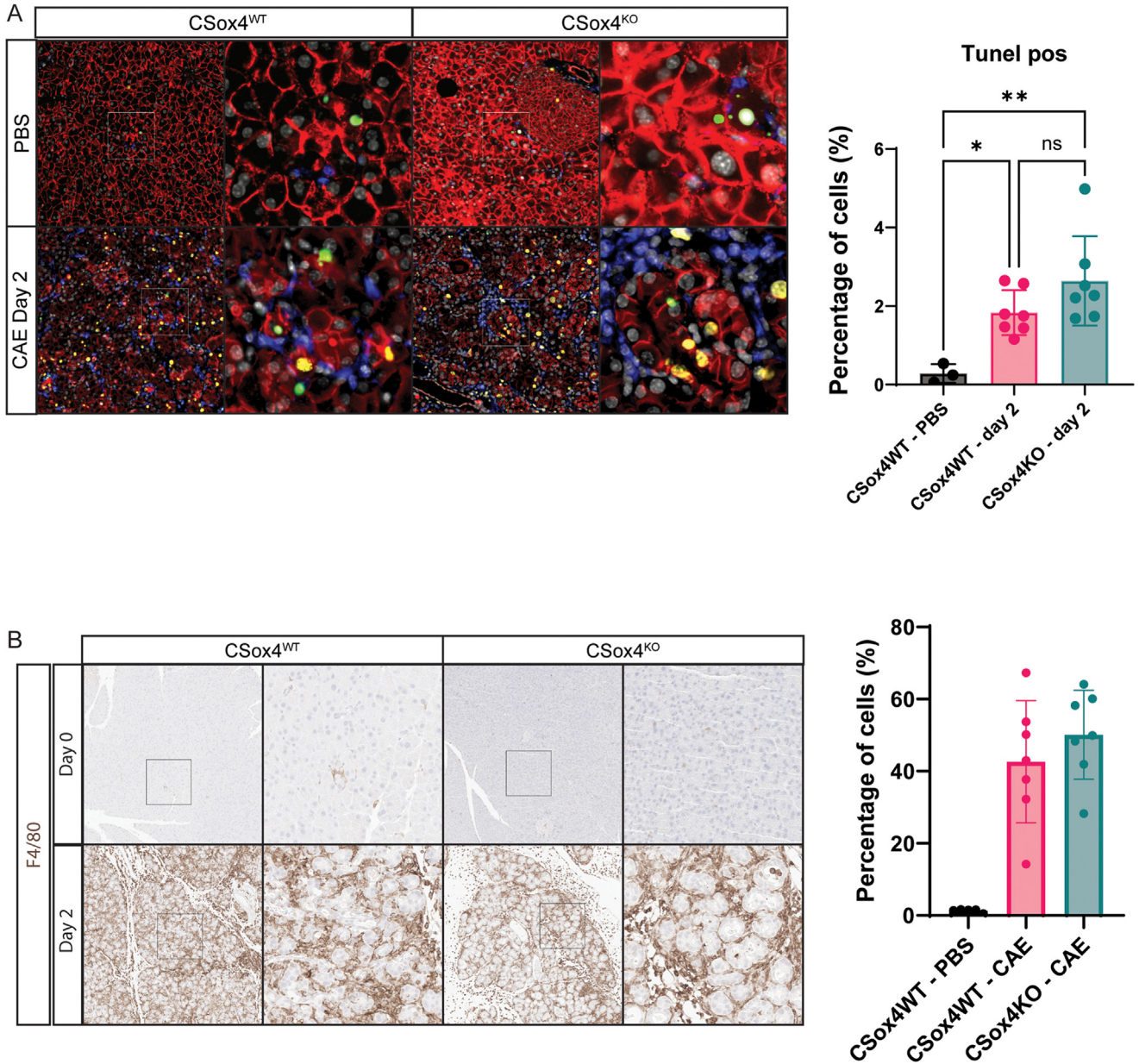
D



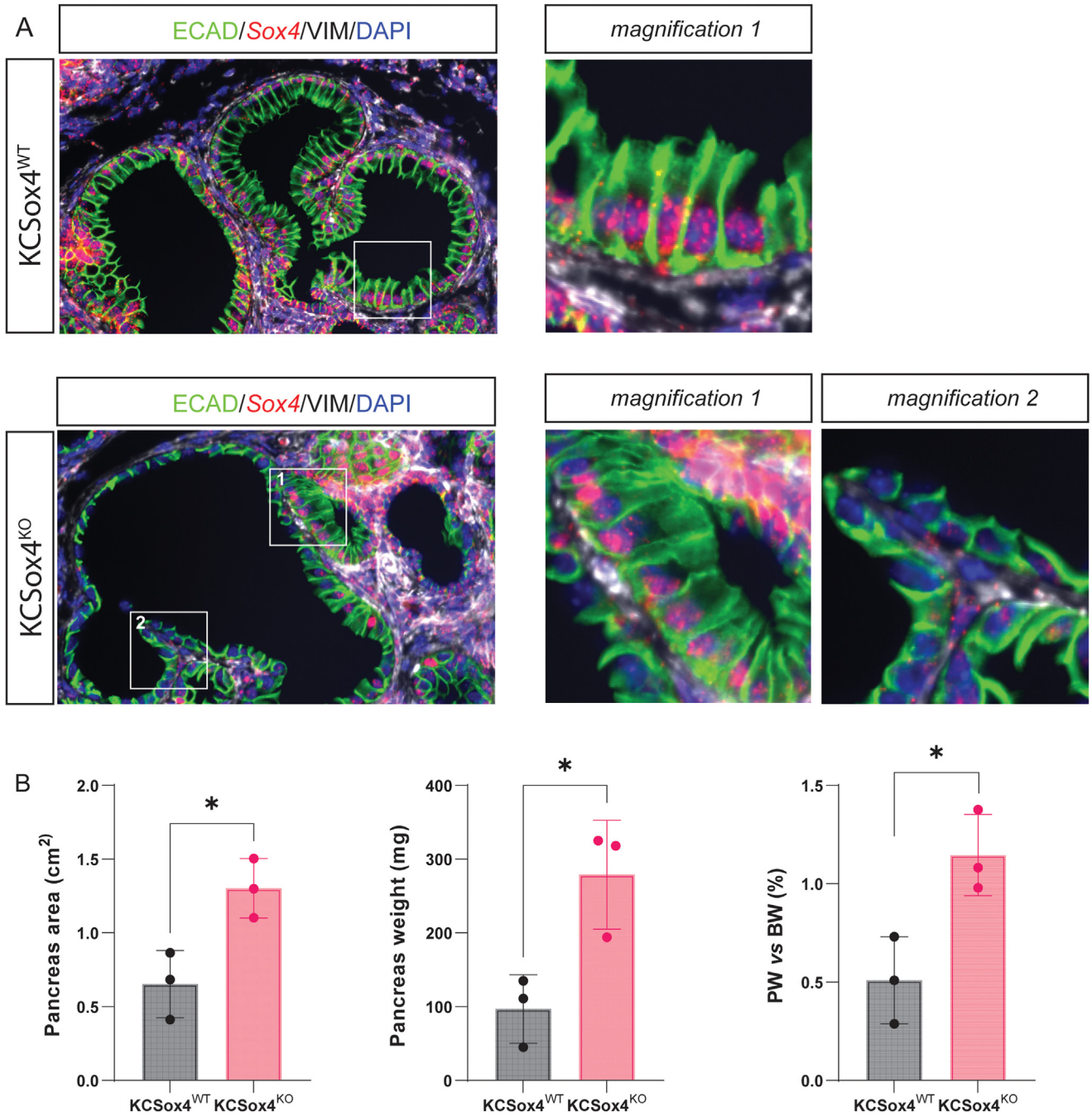
E



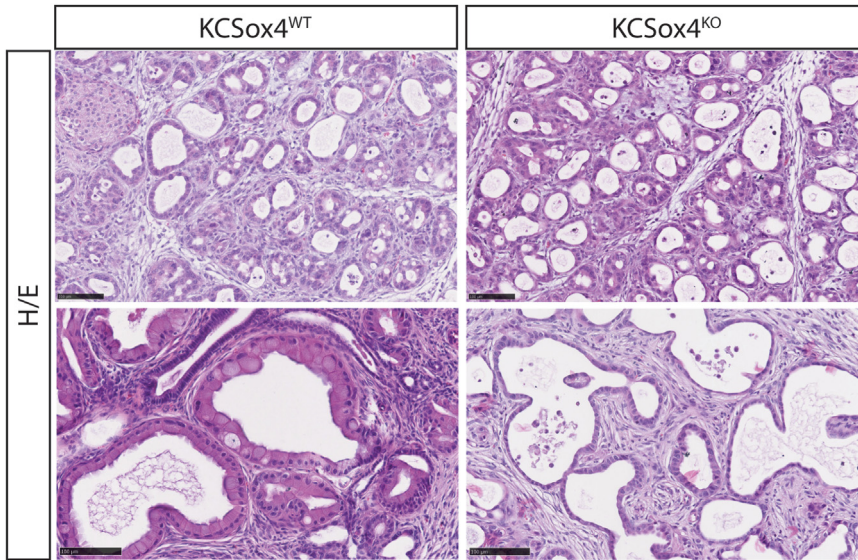
Supplementary Figure 7. (continued).



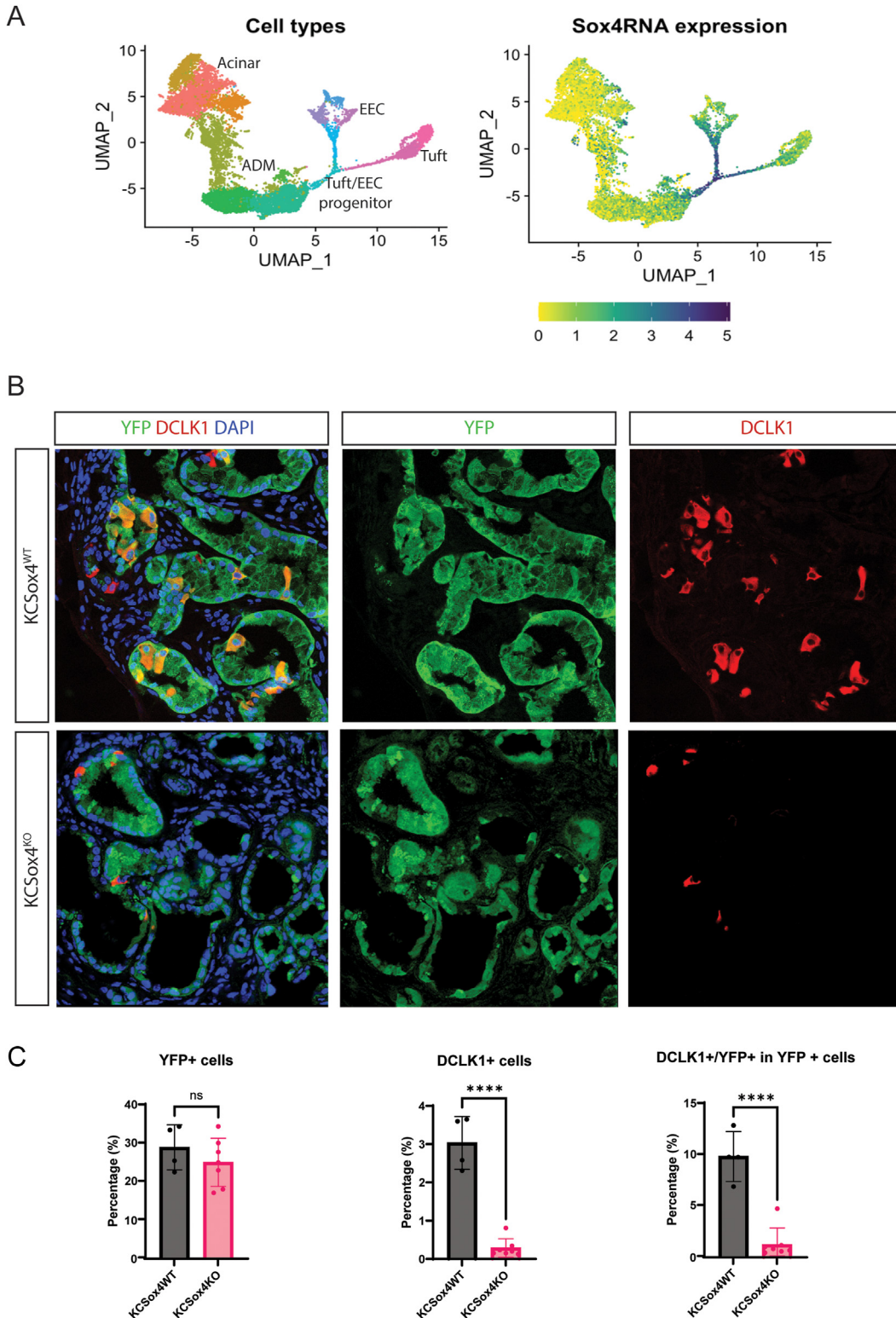
Supplementary Figure 8. Loss of *Sox4* does not result in increased cell death. (A) Immunofluorescence and TUNEL assay. We assessed the number of green apoptotic (TUNEL⁺) and red epithelial cells (ECAD⁺) in CSox4^{KO} and CSox4^{WT} mice (n > 3). Vimentin⁺ stromal cells are labeled in *blue*. No statistical differences observed between CSox4^{KO} and CSox4^{WT} mice at day 2. (B) DAB staining for F4/80. We quantified the number of F4/80⁺ macrophages in CSox4^{KO} and CSox4^{WT} mice at day 2 post caerulein. No statistical differences observed between CSox4^{KO} and CSox4^{WT} mice at day 2 post caerulein. *P < .05, **P < .01. CAE, caerulein; ns, not significant by Mann-Whitney test; TUNEL, terminal deoxynucleotidyl transferase-mediated deoxyuridine triphosphate nick-end labeling.



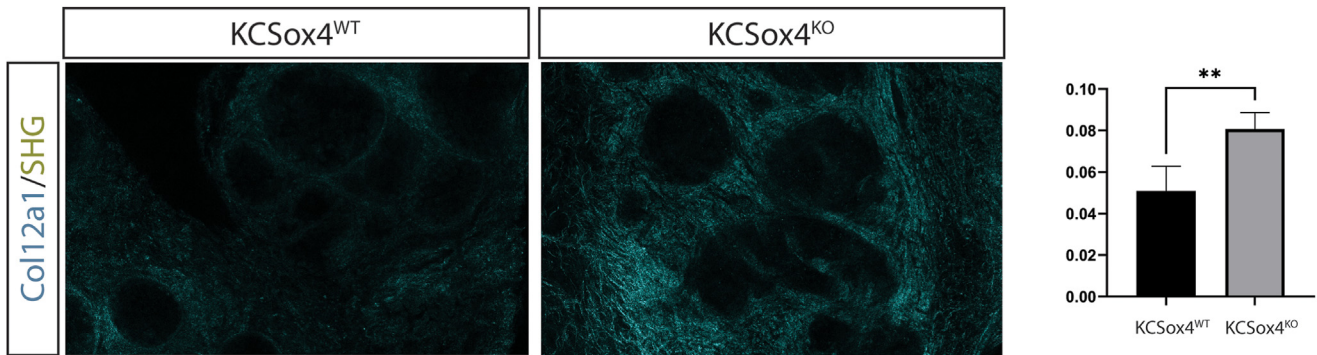
Supplementary Figure 9. Characterization of precancerous lesions of KCSox4^{KO} compared to KCSox4^{WT} mice. (A) We confirmed the conditional KO of Sox4 in acinar cells by ISH and immunofluorescence staining with markers of epithelial cells. Most acinar-derived cells showed loss of Sox4 in KCSox4^{KO} compared to KCSox4^{WT}. We observed cuboidal epithelial cells that remained Sox4-positive, indicating that they escaped cre-mediated recombination of the Sox4 allele. Original magnification, 63 \times . (B) Pancreatic area and pancreas weight were measured 21 days after the injection of caerulein in KCSox4^{WT} and KCSox4^{KO} mice, and we observed a significant increase in the conditional KO for both measures. Statistical tests performed are unpaired 2-tailed Student *t* tests comparing KO with WT samples. *P* values are indicated as **P* < .05. Data are represented as mean \pm standard deviation. Experiments were performed in at least 3 mice. DAPI, 4',6-diamidino-2-phenylindole.



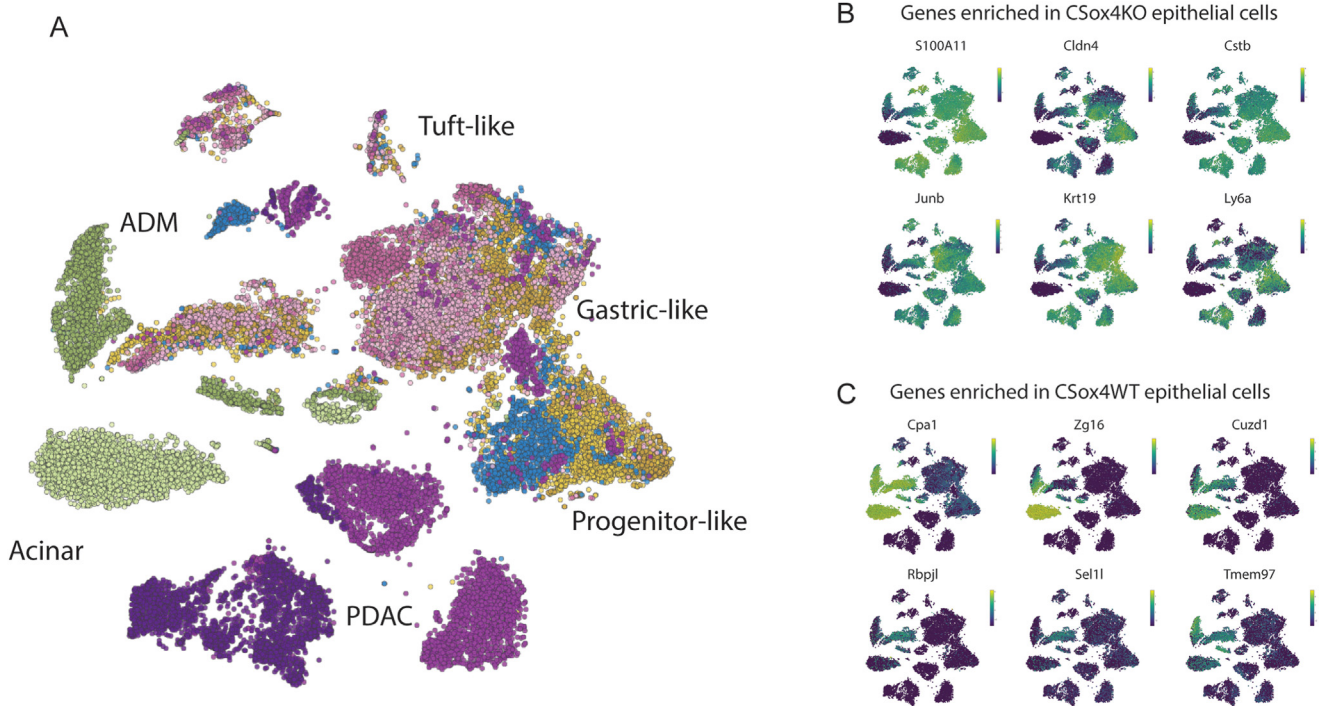
Supplementary Figure 10. Morphometric analysis of precancerous lesions. We performed morphometric analysis of lesions in $KCSox4^{KO}$ compared to $KCSox4^{WT}$ pancreas 21 days after the injection of caerulein. We observed a preponderance of columnar epithelial cells in $KCSox4^{WT}$ compared to mostly cuboidal epithelial cells in $KCSox4^{KO}$ mice, which resulted in a smaller lumen in $KCSox4^{KO}$ compared to $KCSox4^{WT}$ pancreas. At higher magnification, all lesions had basally oriented and uniform nuclei. *Scale bar*, 100 μm . H/E, hematoxylin and eosin.



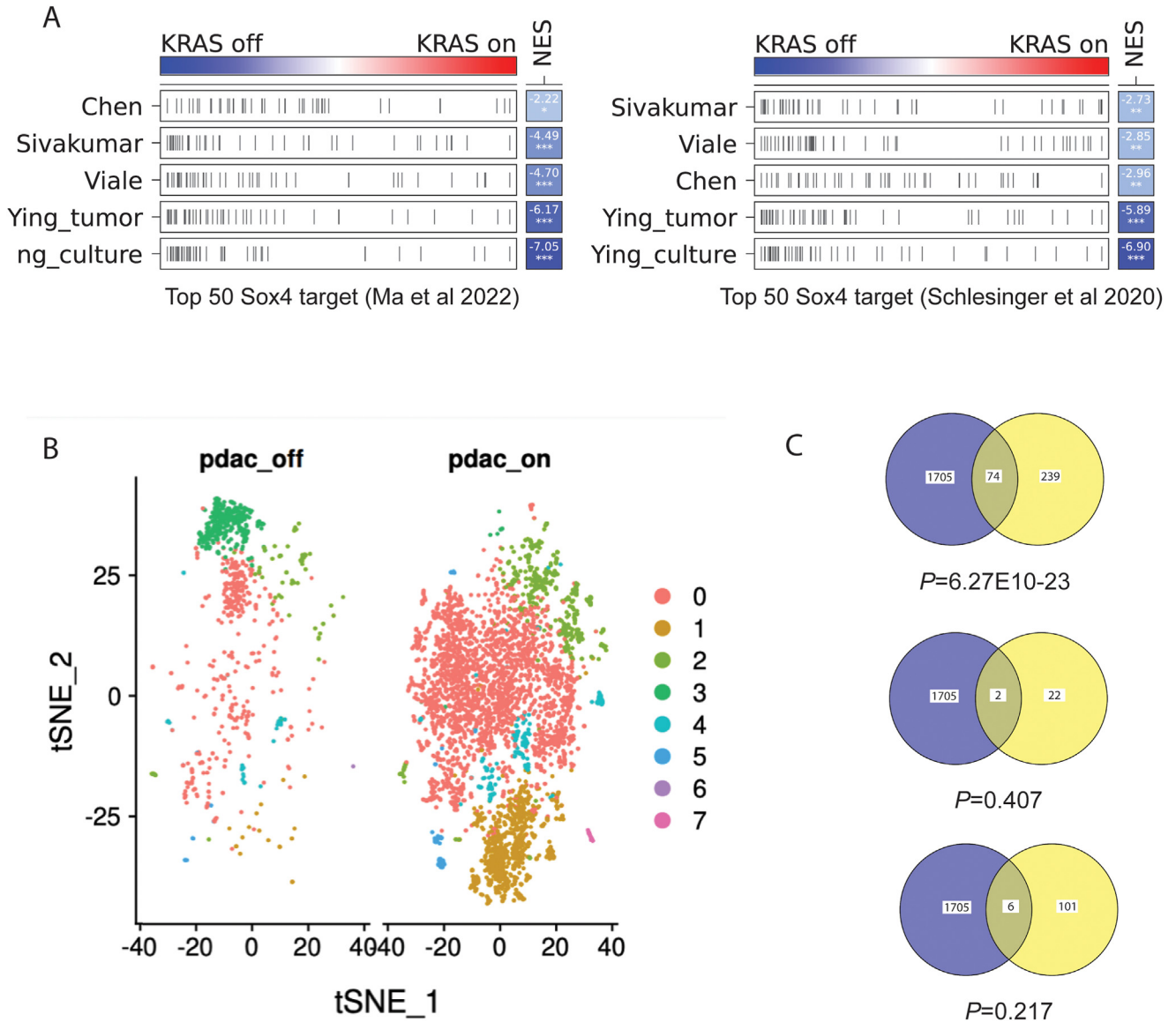
Supplementary Figure 11. Sox4 is necessary for the specification of acinar-derived tuft cells and mucin-producing cells. (A) Expression of Sox4 overlaid on the UMAP of acinar-derived cells in an experimental model of chronic pancreatitis (from Ma et al⁶⁴). (B) Sox4 is required for the specification of acinar-derived tuft cells. Immunofluorescence staining (DAPI in blue, YFP in green, and Dclk1 in red), labeling with YFP the positively recombined acinar cells and with Dclk1 the tuft cells present in the epithelium in tissues collected 21 days after induction of injury with caerulein in KCSox4^{WT} and KCSox4^{KO} mice. (C) Quantification of the percentage of YFP-positive, Dclk1-positive and double-positive cells in lesions in the immunofluorescence in B (n ≥ 3). Data are represented as mean ± standard deviation. Statistical tests performed were unpaired 2-tailed Student t tests. P values are indicated as *P < .05, **P < .01, ***P < .001, ****P < .0001. Original magnification, 40×. DAPI, 4',6-diamidino-2-phenylindole; EEC, enteroendocrine cell; ns, not significant; UMAP, uniform manifold approximation and projection.



Supplementary Figure 12. Loss of Sox4 results in the increased deposition of collagen. We performed immunofluorescence analysis of decellularized tissue from KCSox4^{WT} and KCSox4^{KO}. Decellularized tissue from KCSox4^{KO} mice revealed a higher deposition of collagen XII around the epithelial regions as well as a visible linearization of collagens, suggesting an increased desmoplastic reaction in these lesions. *P* values are indicated as ***P* < .01. Original magnification, 40 \times .



Supplementary Figure 13. Sox4 KO shifts epithelial cells toward malignancy. (A) UMAP plots of scRNAseq profiles of mouse epithelial cells at different stages of PDAC progression from normal acinar cells. (B, C) UMAP plots labeled by cell state and colored by the expression level of genes enriched in CSox4^{KO} (B) and CSox4^{WT} (C). Loss of Sox4 results in the up-regulation of genes associated with late metaplasia and neoplasia. UMAP, uniform manifold approximation and projection.



Supplementary Figure 14. Ablation of oncogenic Kras signaling results in the emergence of a cell population enriched with Sox4 expression and Sox4 targets. (A) We performed gene set enrichment analysis of SOX4-inferred targets with several independent molecular signatures of KRASG12D-depleted tumors. Gene sets are ordered by NES. False discovery rate, <math><0.05</math>. *-/-) before and after doxycycline removal from the drinking water. Ablation of oncogenic Kras signaling results in the emergence of a new population (cluster 3) denoted by the expression of Sox4 and markers of acinar-derived metaplastic cells. (C) Overlap between Sox4 targets and the list of genes enriched in cluster 3 and other clusters of cells identified in the scRNAseq data. Hypergeometric test. NES, normalized enrichment score; tSNE, t -distributed stochastic neighbor embedding.